Band-Limited Impulse Response Estimation Performance

Corentin Lubeigt[a,b,*], Lorenzo Ortega[a,c], Jordi Vilà-Valls[b], Eric Chaumette[b]

[a] *TéSA, 7, Boulevard de la Gare, 31500, Toulouse, France*
[b] *ISAE-SUPAERO, 10, Avenue Edouard Belin, 31055, Toulouse, France*
[c] *IPSA, 40, Boulevard de la Marquette, 31000, Toulouse, France*

Abstract

When a signal is strongly distorted by a reflecting surface, the surface can be seen as a filter whose impulse response is convoluted with the incident signal. Depending on the application, it can be useful to estimate this impulse response in order to either compensate or interpret it. When it comes to estimation, a performance lower bound should be computed in order to better understand the performance limits of the observation model at hand. Hence, a first contribution of this work is to provide an easy-to-use closed-form Cramér-Rao bound for the proposed signal model. The validation process of this lower bound raises the problem of the size, generally unknown, of the impulse response to be estimated. A second contribution of this study is then to provide adapted theoretical and practical tools to determine the size of a given impulse response along with its estimation.

Keywords: Time-delay and Doppler estimation; Cramér-Rao bound; maximum likelihood; band-limited signals; impulse response estimation; FIR length; GNSS remote sensing.

1. Introduction

In wireless, satellite and radiocommunication systems, a signal often bounces over reflecting surfaces before reaching a receiver. It can be on purpose as in remote sensing applications (radar, reflectometry, lidar, etc.) or undesired as in digital communications systems in urban canyons [1]. This phenomenon also occurs in acoustics where reverberation affects music and speech [2].

Depending on the signal bandwidth and the reflecting surface features (roughness, reflectivity, etc.), the reflected signal can be significantly distorted. In the case of remote sensing application, this distortion may contain information regarding the reflecting surface but for digital communications systems, it usually lead to performance deterioration, which has to be compensated for through channel equalization blocks. Either way, there is a strong motivation to better understand the signal distortion.

*Corresponding author
Email address: corentin.lubeigt@tesa.prd.fr (Corentin Lubeigt)

Classically, the distorted signal can be modeled as the convolution between the non-distorted signal and the impulse response of a reflecting surface or a propagation channel [3, 4]. From this point of view, the reflecting surface, or the propagation channel, behaves as a filter whose parameters depends on its features.

As an example, the Global Navigation Satellite Systems (GNSS) signals are more and more exploited as signals of opportunity to perform GNSS Reflectometry (GNSS-R). When the GNSS signal bounces from a reflected surface such as the sea surface, it is more or less distorted depending on the sea state. In particular, the waves height changes the cross-correlation function from a nice and symmetrical triangle to an asymmetric triangle with a long trailing edge [5].

In short, observing the impulse response of the sea state (in terms of size and energy distribution) would allow users to i) evaluate the sea state based on the size of the reflecting surface, ii) classify different reflecting surfaces and, iii) using equalization techniques, better estimate the delay of the received signal which is part of the altimetry product in GNSS-R. These applications can easily be transpose to propagation channel estimation and equalization [6] and to radar, sonar or lidar.

In the process of estimating the impulse response along with the signal parameters (time-delay and Doppler frequency), it is important to know the absolute limit, in the mean square error (MSE) sense, an estimator can reach. A typical tool to account for this absolute limit is the Cramér-Rao bound (CRB) which provides the minimum achievable accuracy in terms of MSE of any unbiased estimator. The CRB for the estimation of an attenuated, time delayed and distorted by a Doppler frequency has been widely studied for wideband [7, 8] and narrowband [9, 10] band-limited signals. The dual source case, without any constraints between the sources has also recently been covered [11] for narrowband band-limited signals. Constrained multi-sources CRB have already been derived for multilayer structures [12] and, more recently for the case of an extended target [13, 14]. However, in this last reference, the authors resort to approximations to evaluate the CRB. Thus, to the best of the authors' knowledge, an easy-to-use, exact expression of the CRB for the estimation of the impulse response of a signal cannot be found in the literature.

The signal model that results from the convolution between the impulse response and the incident signal can be seen as a conditional signal model (CSM) which has interesting properties in terms of convergence of the MSE of the corresponding maximum likelihood estimator (MLE): indeed, in the asymptotic regime, that is, when the number of samples is large [15] or when the signal-to-noise ratio is is large [16], the MLE of a CSM is known to behave as an efficient estimator: it is unbiased and its MSE is equal to the CRB. Such properties can help validate any CRB expression by comparing them to the estimated MSE of the MLE.

The estimation of the size of the received impulse response can be regarded as a simplified case of the more general estimation problem with an unknown number of sources. In the literature, many ways were developed to tackle this signal detection problem. In high resolution arrays, the number of sources is estimated based on the study of the eigenstructure of the observations covariance matrix with information-theoretic criterion to minimize [17] such as the Akaike Information Criterion (AIC) [18] or the Minimum Descriptive Length

(MDL) [19, 20]. These criteria may be simplified considering the relevancy of the parameters to estimate [21]. It can also be done by performing series of hypothesis tests with bootstrapping [22] or resorting to the Benjamini-Hochberg procedure [23, 24]. Other studies propose a solution based on random matrix theory [25] or subspace consideration [26, 27].

The aim of this contribution is then to start from an extended target signal model seen as a convolution between the transmitted signal and the impulse response of a target or reflecting surface. First, assuming the size of the impulse response known, that is the number of pulses, a closed-form expression of the CRB for the estimation of joint delay-Doppler and impulse response coefficients is derived and validated based on the properties of the corresponding MLE. Then, the question of the unknown size of the impulse response is addressed with a theoretical analysis of a misspecified number of pulses on the overall estimation performance. This discussion suggests two approaches to tackle the detection problem at hand and two corresponding detection strategies are proposed to determine the number of pulses.

The rest of this paper is organized as follows: In Section 2, the signal model under study is presented. The corresponding CRB is derived in Section 3 which is validated through numerical simulations in Section 3.3.3. Finally, a discussion regarding ways to determine the number of pulses of the impulse response, and its impact on the overall estimation performance, is drawn in Section 4. Section 5 concludes this study.

2. Signal Model

In this study, a transmitter T is emitting a band-limited signal $s(t)$ with bandwidth B, over a carrier frequency f_c. This band-limited signal can be expressed as follows,

$$s(t) = \sum_{n=N_1'}^{N_2'} s\left(\frac{n}{F_s}\right) \mathrm{sinc}\left(\pi F_s\left(t - \frac{n}{F_s}\right)\right) \quad \mathrm{FT}\{s(t)\}(f) \ , \ S(f) = \frac{1}{F_s}\sum_{n=N_1'}^{N_2'} s\left(\frac{n}{F_s}\right) e^{-j2\pi n \frac{f}{F_s}}, \ -\frac{B}{2} \leq f \leq \frac{B}{2}, \quad (1)$$

where $\mathrm{sinc}(\cdot)$ is the sine cardinal function, f the frequency, $F_s \geq B$ is the sampling frequency, N_1', N_2' are in Z with $N_1' < N_2'$ and refers to the time-frequency pair. The signal travels from T to a reflecting surface and then to the receiver R. An illustration of this scenario is presented in Figure 1.

Let S be the specular point of the reflecting surface, the transmitter T and S have motions assumed linear and uniform during the duration of observations T_I so that the positions can be described as $\mathbf{p}_{T/S}(t) = \mathbf{p}_{T/S} + \mathbf{v}_{T/S} \cdot t$ where $\mathbf{p}$ and $\mathbf{v}$ are the position and velocity vectors, respectively, and t is the time variable. With this assumption, the distance between T and S is classically approximated by a first order distance-velocity model [28],

$$\|\mathbf{p}_{TS}(t)\|^2 \ , \ \|\mathbf{p}_S(t) - \mathbf{p}_T(t - \tilde{\tau}(t))\|^2 = c\tilde{\tau} \approx d + vt \quad (2)$$

$$\tilde{\tau}(t) \approx \tau_S + bt, \ \tau_S = \frac{d}{c}, \ b = \frac{v}{c}, \quad (3)$$

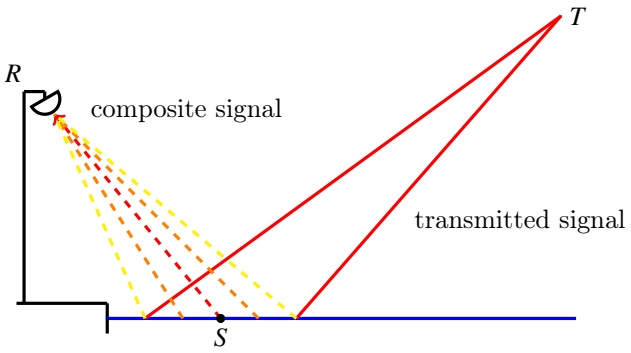

Figure 1: Illustration of the problem

where d is the absolute distance between T and S at instant $t = 0$, v is the radial velocity between T and S, τ is the time delay due to the propagation path, $(1 - b)$ is the dilatation induced by the Doppler effect and c is the speed of light in vacuum. From (3), the complex analytic signal at the point S can be written as,

$$x_S(t) = \rho_S e^{j\tilde{\phi}_S} s\left((1 - b_S)(t - \tau_S)\right) e^{j\omega_c(1-b_S)(t-\tau_S)}, \tag{4}$$

where $\omega_c = 2\pi f_c$, $\boldsymbol{\eta}_S = [\tau_S, b_S]^T$, ρ_S and $\tilde{\phi}_S$, the amplitude (strictly positive) and the phase of the complex coefficient induced by propagation characteristics (fading, scintillation, etc). A simplification of the model can be obtained with the narrowband hypothesis [28]. If one considers that the product $B{\cdot}T_I$ (where T_I is also called the coherent integration time for the considered observation model) is smaller than the inverse Doppler term c/v, then the Doppler effect on the baseband signal $s(t)$ can be neglected: $s((1 - b)(t - \tau)) \approx s(t - \tau)$ ([29, ch.9]). The complex analytic signal at the point S is then written as (with $\phi_S = \tilde{\phi}_S - \omega_c(1 + b_S)\tau_S$),

$$x_S(t) \approx x(t)e^{j\omega_c t} = \left(\rho_S e^{j\phi_S} s\left(t - \tau_S\right) e^{-j\omega_c b_S(t-\tau_S)}\right) e^{j\omega_c t}. \tag{5}$$

The reflecting surface is a complex object that distorts the signal $x_S(t)$, and that can be characterized by its impulse response $h(t)$. The output of such a reflection, expressed at the specular point S, is the convolution product $(*)$ between the input and $h(t)$,

$$y_S(t) = h(t) * x_S(t). \tag{6}$$

Similarly to [13], the impulse response is modelled as a series of echoes regularly separated by a fixed time interval which is the sampling period $T_s = 1/F_s$ (which simply results from the Fourier Series of the surface frequency transfer function). Consequently, the impulse response can be written as a sum of delayed and

attenuated Dirac functions,

$$h(t) = \sum_{p=1}^{P} \tilde{\rho}_p e^{j\tilde{\phi}_p} \delta(t - (p-1)T_s), \tag{7}$$

where P is the number of consecutive echoes in the impulse response of the reflecting surface. The resulting signal expressed at the receiver R after the reflection is then written as follows,

$$y_R(t) = \sum_{p=1}^{P} \tilde{\rho}_p e^{j\tilde{\phi}_p} d(t - (p-1)T_s; \boldsymbol{\eta}, \rho, \phi) e^{j\omega_c (t-(p-1)T_s)} \tag{8}$$

$$= \left(\sum_{p=1}^{P} \rho_p e^{j\phi_p} s_p(t; \boldsymbol{\eta}) \right) e^{j\omega_c t}, \tag{9}$$

with $\boldsymbol{\eta} = [\tau, b]^T$, τ is the sum of the time delay due to the propagation from T to S and the one due to the propagation from S to R, b is the resulting Doppler stretch after the reflection, $\rho_p \ , \ \rho\tilde{\rho}_p$ and $\phi_p \ , \ \phi + \tilde{\phi}_p - \omega_c(p-1)T_s$, $\rho e^{j\phi}$ being the complex amplitude associated to the transmission from T to R via a perfect specular reflection in S, and with $\tau_p = \tau + (p-1)T_s$ yielding,

$$s_p(t; \boldsymbol{\eta}) \ , \ s\left(t - \tau_p\right) e^{-j\omega_c b(t-\tau_p)}. \tag{10}$$

The baseband output of the receiver's Hilbert filter with bandwidth F_s containing the reflected signal is then given by,

$$y(t) = y_R(t) e^{-j\omega_c t} = \sum_{p=1}^{P} d_p(t; \boldsymbol{\eta}, \rho_p, \phi_p) + w(t), \tag{11}$$

$$d_p(t; \boldsymbol{\eta}, \rho_p, \phi_p) \ , \ \rho_p e^{j\phi_p} s_p(t; \boldsymbol{\eta}), \tag{12}$$

where $w(t)$ is a zero-mean additive complex Gaussian noise with variance σ_n^2. Now if one considers the acquisition of $N = N_2 - N_1 + 1$ ($N_1 \ll N_1'$, $N_2 \gg N_2'$) samples at a sampling frequency F_s, the resulting discrete signal appears as a CSM,

$$\mathbf{y} = \mathbf{A}_P(\boldsymbol{\eta})\boldsymbol{\alpha} + \mathbf{w}, \ \mathbf{w} \sim \mathcal{CN}(0, \sigma_n^2 \mathbf{I}_N), \tag{13}$$

with, for $n \in [N_1, N_2]$ and $p \in [1, P]$,

$$\mathbf{y}^T = (\ldots, y(nT_s), \ldots), \ \mathbf{A}_P(\boldsymbol{\eta}) = \left[\ldots, \mathbf{s}_p(\boldsymbol{\eta}), \ldots\right], \ \mathbf{s}_p(\boldsymbol{\eta})^T = \left(\ldots, s(nT_s - \tau_p) e^{-j\omega_c b(nT_s - \tau_p)}, \ldots\right),$$
$$\boldsymbol{\alpha}^T \ , \ (\ldots, \alpha_p, \ldots) = (\ldots, \rho_p e^{j\phi_p}, \ldots), \ \mathbf{w}^T = (\ldots, w(nT_s), \ldots).$$

3. Compact CRB for the Joint Delay-Doppler Estimation with a Discrete Impulse Response

3.1. Evaluation of the Fisher Information Matrix

The purpose of this section is to present a new compact CRB for the estimation of the parameters of the CSM (13). These parameters can be presented under the form of a vector $\boldsymbol{\epsilon}^T \ , \ (\sigma_n^2, \bar{\boldsymbol{\epsilon}}^T)$ with $\bar{\boldsymbol{\epsilon}}^T \ , \ (\boldsymbol{\eta}^T, \alpha_1^r, \alpha_1^i, \ldots, \alpha_P^r, \alpha_P^i)$ with, for $p \in [1, P]$, $\alpha_p = \alpha_p^r + j\alpha_p^i$. From its expression in (13) and from the assumption of a zero-mean complex Gaussian white noise, the distribution of the sampled received signal is also Gaussian: $\mathbf{y} \sim \mathcal{CN}(\mathbf{A}_P(\boldsymbol{\eta})\boldsymbol{\alpha}, \sigma_n^2 \mathbf{I}_N)$ and one can apply the Slepian-Bangs formula [30] to evaluate the Fisher Information Matrix (FIM), which is defined as the inverse of the CRB,

$$\mathbf{CRB}_{\boldsymbol{\epsilon}|\boldsymbol{\epsilon}} \ , \ \left(\mathbf{F}_{\boldsymbol{\epsilon}|\boldsymbol{\epsilon}}\right)^{-1}, \tag{14}$$

and,

$$\left[\mathbf{F}_{\boldsymbol{\epsilon}|\boldsymbol{\epsilon}}\right]_{k,l} \ , \ F_{\epsilon_k,\epsilon_l|\boldsymbol{\epsilon}} = \frac{2}{\sigma_n^2}\mathrm{Re}\left\{\left(\frac{\partial \mathbf{A}_P(\boldsymbol{\eta})\boldsymbol{\alpha}}{\partial \epsilon_k}\right)^H \left(\frac{\partial \mathbf{A}_P(\boldsymbol{\eta})\boldsymbol{\alpha}}{\partial \epsilon_l}\right)\right\} + \frac{N}{\sigma_n^4}\frac{\partial \sigma_n^2}{\partial \epsilon_k}\frac{\partial \sigma_n^2}{\partial \epsilon_l}, \tag{15}$$

where k and l denotes the row and column index. The noise variance being independent from the other parameters [31], the FIM is simply,

$$\mathbf{F}_{\boldsymbol{\epsilon}|\boldsymbol{\epsilon}} = \begin{bmatrix} F_{\sigma_n^2|\boldsymbol{\epsilon}} & \mathbf{0}_{1,2P+2} \\ \mathbf{0}_{2P+2,1} & \mathbf{F}_{\bar{\boldsymbol{\epsilon}}|\boldsymbol{\epsilon}} \end{bmatrix}, \tag{16}$$

where $F_{\sigma_n^2|\boldsymbol{\epsilon}} = N/\sigma_n^4$, which is a known result, and $\mathbf{F}_{\bar{\boldsymbol{\epsilon}}|\boldsymbol{\epsilon}}$ is the FIM for the estimation of the delay-Doppler along with the P echoes of the discrete impulse response. This FIM can be written as follows,

$$\mathbf{F}_{\bar{\boldsymbol{\epsilon}}|\boldsymbol{\epsilon}}(\boldsymbol{\epsilon}) = \frac{2F_s}{\sigma_n^2}\mathrm{Re}\left\{\mathbf{Q}\mathbf{W}^{\delta}\mathbf{Q}^H\right\}, \tag{17}$$

with $\mathbf{Q}$ defined in (A.2) and $\mathbf{W}^{\delta}$ defined as,

$$\mathbf{W}^{\delta} \ , \ \begin{bmatrix} \mathbf{W}_1^{\delta} & \mathbf{W}_2^{\delta H} & \mathbf{W}_3^{\delta H} \\ \mathbf{W}_2^{\delta} & \mathbf{W}_{2,2}^{\delta} & \mathbf{W}_4^{\delta H} \\ \mathbf{W}_3^{\delta} & \mathbf{W}_4^{\delta} & \mathbf{W}_{3,3}^{\delta} \end{bmatrix}, \tag{18}$$

where the different components are $P \times P$ hermitian matrices computed through the baseband signal samples, for p the row index and q the column index in $[1, P]$,

$$\begin{aligned} &\left[\mathbf{W}_1^{\delta}\right]_{p,q} = \frac{1}{F_s}\mathbf{s}^H\mathbf{V}^{\ ,0}(p-q)\mathbf{s}, \ \left[\mathbf{W}_2^{\delta}\right]_{p,q} = \frac{1}{F_s^2}\mathbf{s}^H\mathbf{V}^{\ ,0}(p-q)\mathbf{D}\mathbf{s}, \ \left[\mathbf{W}_3^{\delta}\right]_{p,q} = \mathbf{s}^H\mathbf{V}^{\ ,1}(p-q)\mathbf{s}, \\ &\left[\mathbf{W}_4^{\delta}\right]_{p,q} = \frac{1}{F_s}\mathbf{s}^H\mathbf{D}\mathbf{V}^{\ ,1}(p-q)\mathbf{s}, \ \left[\mathbf{W}_{2,2}^{\delta}\right]_{p,q} = \mathbf{s}^H\mathbf{D}\mathbf{V}^{\ ,0}(p-q)\mathbf{D}\mathbf{s}, \ \left[\mathbf{W}_{3,3}^{\delta}\right]_{p,q} = F_s\mathbf{s}^H\mathbf{V}^{\ ,2}(p-q), \end{aligned} \tag{19}$$

with $\mathbf{s}$ the baseband sample vector defined in (A.15), $\mathbf{D}$ in (A.19), $\mathbf{V}^{,0}(\cdot)$ in (A.17), $\mathbf{V}^{,1}(\cdot)$ in (A.20) and $\mathbf{V}^{,2}(\cdot)$ in (A.22).

Proof. see Appendix A.1

Remark that an equivalent expression can be found by considering the vector of unknown parameters $\boldsymbol{\zeta}^T = (\sigma_n^2, \bar{\boldsymbol{\zeta}}^T)$ and $\bar{\boldsymbol{\zeta}}^T = (\boldsymbol{\eta}^T, \boldsymbol{\rho}^T, \boldsymbol{\phi}^T)$ where for $p \in [1, P]$, $\boldsymbol{\rho}^T = (\ldots, \rho_p, \ldots)$ and $\boldsymbol{\phi}^T = (\ldots, \phi_p, \ldots)$. The only change in the computation is in the matrix $\mathbf{Q}$ but the FIM can be written as in (17) (see Appendix A.2). For the rest of this work, the vector of unknown parameters may change from $\boldsymbol{\epsilon}$ to $\boldsymbol{\zeta}$ depending on the need.

3.2. Comparison with Existing Results

The obtained FIM can be compared to existing formulations for similar problems. First, if $P = 1$, then, remarking that $\mathbf{V}^{,0}(0) = \mathbf{I}_N$,

$$\begin{aligned} W_1^\delta &= \frac{1}{F_s}\mathbf{s}^H\mathbf{s},\ W_2^\delta = \frac{1}{F_s^2}\mathbf{s}^H\mathbf{D}\mathbf{s},\ W_3^\delta = \mathbf{s}^H\mathbf{V}^{,1}(0)\mathbf{s}, \\ W_4^\delta &= \frac{1}{F_s}\mathbf{s}^H\mathbf{D}\mathbf{V}^{,1}(0)\mathbf{s},\ W_{2,2}^\delta = \mathbf{s}^H\mathbf{D}^2\mathbf{s},\ W_{3,3}^\delta = F_s\mathbf{s}^H\mathbf{V}^{,2}(0)\mathbf{s}, \end{aligned} \tag{20}$$

and the resulting FIM characterizes the estimation of the joint delay-Doppler and complex amplitude of a signal, for instance, when no multipath is present. This has been studied in [7, 9] for the GNSS case.

Secondly, if $P = 2$, the resulting FIM represents a two-ray model such as the one studied in [11]. As a reminder, in this previous work, the general expression of the dual source CRB was evaluated for the estimation of following vector of unknowns $\boldsymbol{\xi}^T = [\sigma_n^2, \tau_1, b_1, \rho_1, \phi_1, \tau_2, b_2, \rho_2, \phi_2]$, where there is no relation between τ_1 and τ_2, or between b_1 and b_2. In that case one can evaluate the general expression of this dual source CRB for a range $\tau = \tau_2 - \tau_1$, known as the path separation, and apply a reparameterization to constrain the general CRB to the model used in the this contribution, that is,

$$\tau_1 = \tau = \tau_2 - \tau \text{ and } b_1 = b_2 = b. \tag{21}$$

Note that when $\tau = 1/F_s$, the resulting reparameterized FIM should match the FIM evaluated in (17) when considering the vector of unknown parameters $\boldsymbol{\zeta}$ as mentioned at the end of Section 3.1. With the relations in (21), the jacobian corresponding to this reparameterization is,

$$\frac{\partial\boldsymbol{\xi}(\boldsymbol{\zeta})}{\partial\boldsymbol{\zeta}^T} = \begin{bmatrix} \mathbf{e}_1 & \mathbf{e}_2 + \mathbf{e}_6 & \mathbf{e}_3 + \mathbf{e}_7 & \mathbf{e}_4 & \mathbf{e}_8 & \mathbf{e}_5 & \mathbf{e}_9 \end{bmatrix}, \tag{22}$$

where $\mathbf{e}_i$ is the 9-element column unitary vector with zeros everywhere except at the i-th index. Then,

$$\mathbf{F}^r_{\zeta|\zeta}(\boldsymbol{\zeta}) = \left(\frac{\partial \boldsymbol{\xi}(\boldsymbol{\zeta})}{\partial \boldsymbol{\zeta}^T}\right)^T \mathbf{F}_{\xi|\xi}(\boldsymbol{\xi}) \frac{\partial \boldsymbol{\xi}(\boldsymbol{\zeta})}{\partial \boldsymbol{\zeta}^T}, \tag{23}$$

where $\mathbf{F}^r_{\zeta|\zeta}(\boldsymbol{\zeta})$ is the reparameterized FIM, from the CRB expression derived in [11] and the relations (21). To visually validate the consistency between the reparameterized FIM (23) and the work presented in this contribution, a numerical application is proposed using a simple GNSS signal: the GPS L1 C/A signal [32]. This signal consists of a non-return-to-zero (NRZ) line code modulated by a Binary Phase Shift Keying (BPSK) modulation. Its chip rate is 1.023 MHz. In the sequel, the C/A chip corresponds to the chip period of the BPSK, that is about 1μs. Figure 2 presents the τ term of the square root of the inverse of $\mathbf{F}^r_{\zeta|\zeta}$, when τ varies, for three values of F_s. The three points at 1/8, 1/4 and 1/2 C/A chips correspond to the τ term of the square root inverse of the FIM defined in (17). These points are located on their corresponding curves which demonstrates that the CRB expressions derived in this contribution for $P = 2$ are consistent with the existing expressions when applying the constraints defined in (21).

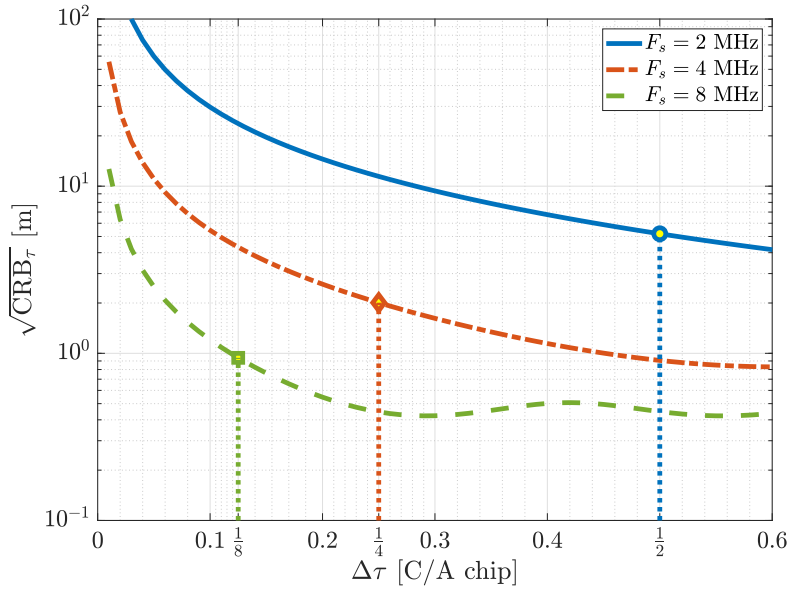

Figure 2: Evolution of the constrained CRB obtained after reparameterization of the general dual source CRB for $F_s = \{2, 4, 8\}$ MHz as a function of the path separation τ expressed in GPS L1 C/A chips. The three points are the evaluation of the CRB derived in this contribution. This figure was obtained for a GPS L1 C/A signal with a noise level $\mathrm{SNR}_{\mathrm{out}}$=33dB, amplitudes $\boldsymbol{\rho}^T = [1, 0.5]$ and phases $\boldsymbol{\phi}^T = [0, 0]$. The vertical axis is multiplied by the speed of light to be converted to meters.

Finally, in order to connect this work to other existing CRB expressions as in [13], recall that in this reference, the authors had to use a Taylor approximation to obtain tractable expressions. Here the expression proposed in (17) is easy to handle thanks to its matrix form and it does not rely on any assumption; it only exploits the Shannon-Nyquist theorem on the representation of band-limited signals. The signal model

presented in this reference is fundamentally different than the signal model (13): in fact, in [13], the authors worked on a signal model that contains the carrier frequency where (13) assumes that the carrier frequency is taken off at the demodulation step. This difference makes it difficult to connect the proposed expression to the results from the literature. As a final comment on the existing expression proposed in [13]: in the numerical results, the authors compared the derived expression to the performance of two estimators, the Oracle estimator that assumed all the amplitudes known and the Wideband Ambiguity Function (WBAF) estimator that assumes a single source in the impulse response. The Oracle estimator, being helped by the knowledge of the amplitudes could have its MSE smaller than the proposed CRB. The WBAF estimator, underestimating the number of sources and then being strongly misspecified, could have a MSE floored at a given value because of a residual bias. None of these two estimators is asymptotically efficient for estimation problem considered by the authors. They could not be used to ensure the expressions validity.

The question of the validation of the CRB expression proposed in this contribution is tackled in the next section where it is compared to the MSE of the MLE that matches the signal model (13).

3.3. Validation and Discussion

3.3.1. Methodology and Considered Scenarios

A way to ensure the validity of the CRB expression derived in Section 3 is to find an efficient estimator for the signal model under study and to evaluate its MSE. Indeed, an efficient estimator is unbiased and with a MSE equal to the CRB. Unfortunately, such an estimator cannot be found for the nonlinear problem under study, and one can only find an estimator with an asymptotic efficiency, for instance the conditional MLE. It has been shown that in its asymptotic regimes, that is, when the SNR is large enough [16] or when the number of samples is large enough [15], the MLE tends to behave as an efficient estimator. The purpose of this section is first to present an implementation of the MLE, and then to apply it to two scenarios in order to obtain an estimate of the MSE, and compare it to the corresponding CRB. In short, if the MLE MSE fits with the CRB, this implies that the derived expression is correct.

The two scenarios considered for this validation are presented in Figure 3a and Figure 3b under the form of amplitude-delay-profiles, similarly to multipath power-delay-profiles that can be found in [33, Fig. 9.14]. Scenario #1 is a simple set of four consecutive decreasing echoes. Scenario #2 is also a set of four consecutive echoes, but with the the second being of amplitude zero.

3.3.2. Maximum Likelihood Estimator

The MLE is a common sense estimator, that is, it consists of selecting the parameters that are the most likely with respect to the samples available. Knowing the probability density function of the signal (13),

$$p(\mathbf{y};\boldsymbol{\epsilon}) = \frac{1}{\left(\pi\sigma_n^2\right)^N} e^{-\frac{1}{\sigma_n^2}\|\mathbf{y}-\mathbf{A}_P\boldsymbol{\alpha}\|^2}, \tag{24}$$

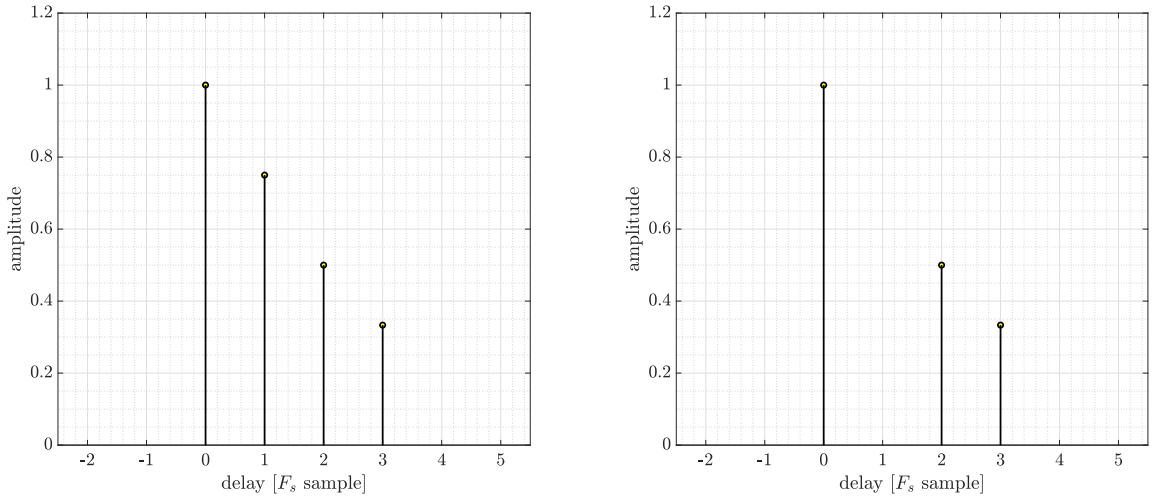

(**a**) Scenario #1 (**b**) Scenario #2

Figure 3: Amplitude-delay-profiles of the scenarios considered. It consists of a set of four consecutive echoes with $\boldsymbol{\rho}_1^T = [1, 3/4, 1/2, 1/3]$ for scenario #1 (**a**) and $\boldsymbol{\rho}_2^T = [1, 0, 1/2, 1/3]$ for scenario (**b**). For these scenario, the sampling frequency is set to $F_s = 4$ MHz.

maximizing (24) is equivalent to minimizing the norm in the exponential function, which can be split into two orthogonal terms with the introduction of the projector over the space formed by the columns of the matrix $\mathbf{A}_P$: $\mathbf{P}_{\mathbf{A}_P} = \mathbf{A}_P \left(\mathbf{A}_P^H \mathbf{A}_P\right)^{-1} \mathbf{A}_P^H$, $\mathbf{P}^{\perp}_{\mathbf{A}_P} = \mathbf{I} - \mathbf{P}_{\mathbf{A}_P}$.

$$\begin{aligned} \|\mathbf{y} - \mathbf{A}_P\boldsymbol{\alpha}\|^2 &= \left\|\mathbf{P}_{\mathbf{A}_P}\left(\mathbf{y} - \mathbf{A}_P\boldsymbol{\alpha}\right)\right\|^2 + \left\|\mathbf{P}^{\perp}_{\mathbf{A}_P}\left(\mathbf{y} - \mathbf{A}_P\boldsymbol{\alpha}\right)\right\|^2 \\ &= \left\|\mathbf{A}_P\left(\left(\mathbf{A}_P^H\mathbf{A}_P\right)^{-1}\mathbf{A}_P^H\mathbf{y} - \boldsymbol{\alpha}\right)\right\|^2 + \left\|\mathbf{P}^{\perp}_{\mathbf{A}_P}\mathbf{y}\right\|^2 . \end{aligned} \tag{25}$$

From the decomposition (25), the expression of the estimated vector $\widehat{\boldsymbol{\epsilon}}$ is simplified; the estimation of the delay-Doppler vector $\widehat{\boldsymbol{\eta}}$ is decoupled from the estimation of the complex amplitudes,

$$\widehat{\boldsymbol{\eta}} = \arg\max_{\boldsymbol{\eta}} \left\|\mathbf{P}_{\mathbf{A}_P(\boldsymbol{\eta})}\mathbf{y}\right\|^2, \ \widehat{\alpha}_p = \left[\left(\mathbf{A}_P^H(\widehat{\boldsymbol{\eta}})\mathbf{A}_P(\widehat{\boldsymbol{\eta}})\right)^{-1}\mathbf{A}_P^H(\widehat{\boldsymbol{\eta}})\mathbf{y}\right]_p , \tag{26}$$

$$\widehat{\alpha}_p^r = \mathrm{Re}\{\widehat{\alpha}_p\}, \ \widehat{\alpha}_p^i = \mathrm{Im}\{\widehat{\alpha}_p\}, \ \widehat{\rho}_p = |\widehat{\alpha}_p|, \ \widehat{\phi}_p^i = \arg\{\widehat{\alpha}_p\}, \tag{27}$$

$$\widehat{\sigma}_n^2 = \frac{1}{N}\left\|\mathbf{P}^{\perp}_{\mathbf{A}_P(\widehat{\boldsymbol{\eta}})}\mathbf{y}\right\|^2 . \tag{28}$$

The projection (26) can be further developed to obtain an easy to implement formulation given in Appendix B. For the rest of this contribution, the MLE of an impulse response, parameterized by the number of pulses P and the regular interval between each pulse τ_p, will be denoted IR-MLE(P, τ_p). In this work, the input of the estimator is the number of consecutive sources to estimate P, which is assumed to be known in this section, each sources being separated by T_s as it is presented in the signal model (13), that is, the

implemented estimator will be IR-MLE(P, T_s).

3.3.3. Numerical Results

The following figures show the root CRB and the root MSE (RMSE) of the MLE for 1000 Monte Carlo realizations, as a function of the SNR at the output of the matched filter. The deterministic parameters are set as follows: $\tau = 0$, $F_d = bf_c = 200$ Hz, $\boldsymbol{\alpha}$ depends on the scenario under consideration (see Figure 3a and 3b for the amplitudes), the phase of the echoes, $\boldsymbol{\phi}$, is a set of four random phases. The $\mathrm{SNR}_{\mathrm{out}}$ is defined with respect to (w.r.t.) the first echo ρ_1,

$$\mathrm{SNR}_{\mathrm{out}} \ , \ \frac{\rho_1^2 \mathbf{s}^H \mathbf{s}}{\sigma_n^2}. \tag{29}$$

For all the simulations, a GPS L1 C/A signal, coherently integrated for $T_I = 1$ms at a sampling frequency $F_s = 4$ MHz was considered.

Scenario #1. For this first scenario, the true values of the phases were randomly picked. The considered values for the simulations were set to $\boldsymbol{\phi}_1^T = [334°, 37°, 114°, 355°]$. Figure 4a and Figure 4b present the RMSE for the estimation of the delay τ and the Doppler frequency F_d of the IR-MLE(4,T_s). In Figure 4a, one can observe the threshold region (where the RMSE reaches the square-root CRB) at $\mathrm{SNR}_{\mathrm{out}} = 27$ dB. For the Doppler frequency, its RMSE is equal to the corresponding bounds for the range of $\mathrm{SNR}_{\mathrm{out}}$ considered here. Figure 4c presents the RMSE for the four echoes complex amplitudes estimations along with their corresponding bounds. From this figure, one can first see that the RMSE satisfyingly follow the square-root CRB, which validates the proposed CRB expressions.

Scenario #2. In this second scenario, the true values of the phases are $\boldsymbol{\phi}_2^T = [45°, \mathrm{N/A}, 184°, 328°]$, the second phase being not applicable because the second amplitude is equal to 0. Figure 5a and Figure 5b correspond to the RMSE of the IR-MLE(4,T_s) for the estimation of the delay and Doppler frequency. For both parameters the RMSE does reach the square-root CRB, which, again, is in accordance with theory. Figure 5c, presents the RMSE for the estimation of the four amplitudes. In this figure, one can see a good fit of the RMSE on the corresponding CRB.

4. Determination of the Number of Pulses

So far, the number of pulses that described the impulse response was assumed known. However this number is often unknown and can vary in time. In this section, a theoretical analysis of the impact of under- and overestimating the number of pulses is first proposed in Section 4.1. This study suggests two different strategies to determine the number of pulses. Both strategies are then detailed with two proposed

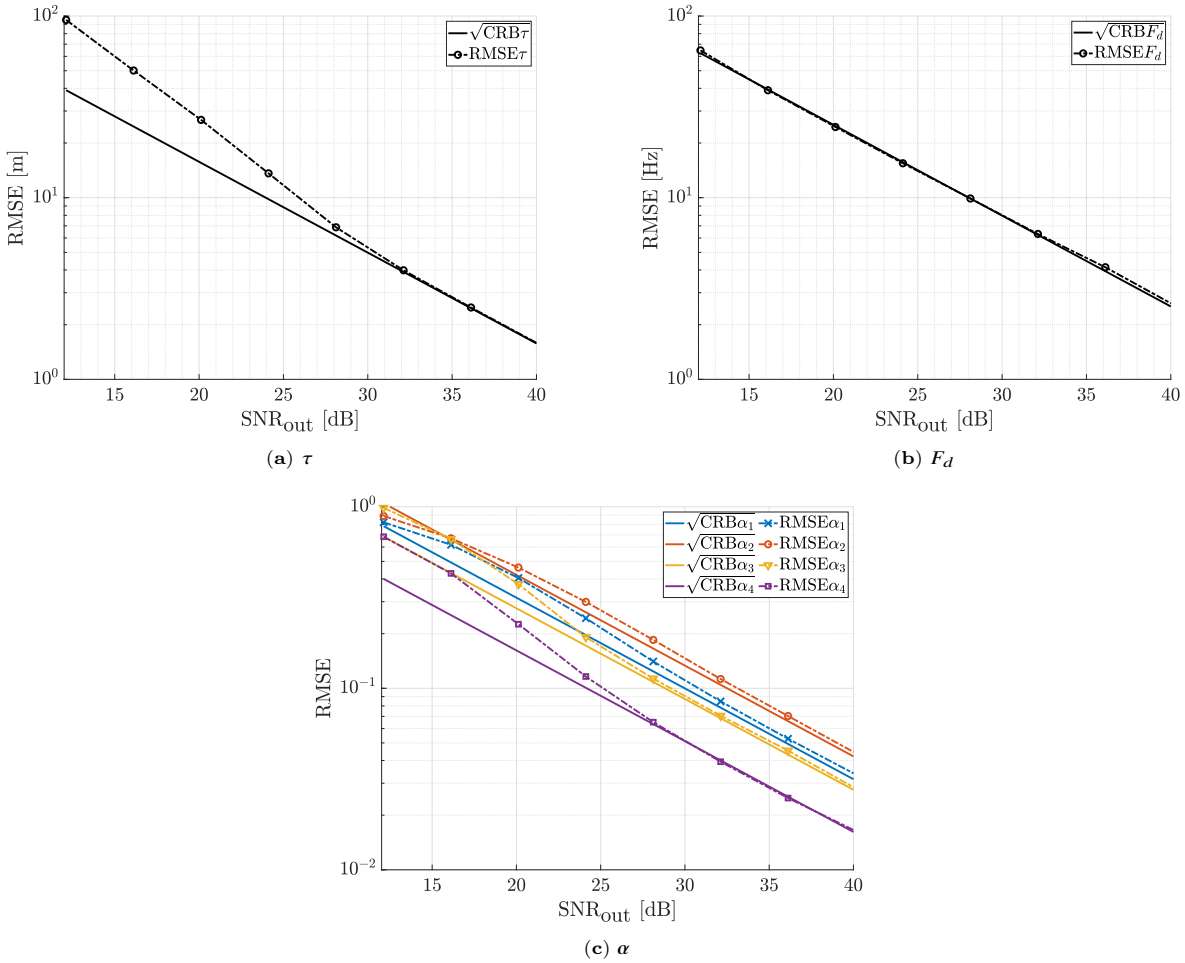

Figure 4: Scenario #1: RMSE for the estimation of the parameters with IR-MLE(4,T_s).

procedures in Section 4.2 and in Section 4.3. For each procedure, numerical examples are presented to support theoretical results.

4.1. Theoretical Analysis

Let $h(t)$ be a band-limited causal impulse response with a finite number of pulses P. This impulse response can be written as,

$$h(t) = \sum_{p=1}^{P} \alpha_p \delta\left(t - (p-1)T_s\right) + \sum_{q=1}^{\infty} \alpha_{P+q} \delta\left(t - (P+q-1)T_s\right), \quad \begin{cases} \alpha_1 < 0 \\ \alpha_P < 0 \\ \alpha_{P+q} = 0 \end{cases}, \tag{30}$$

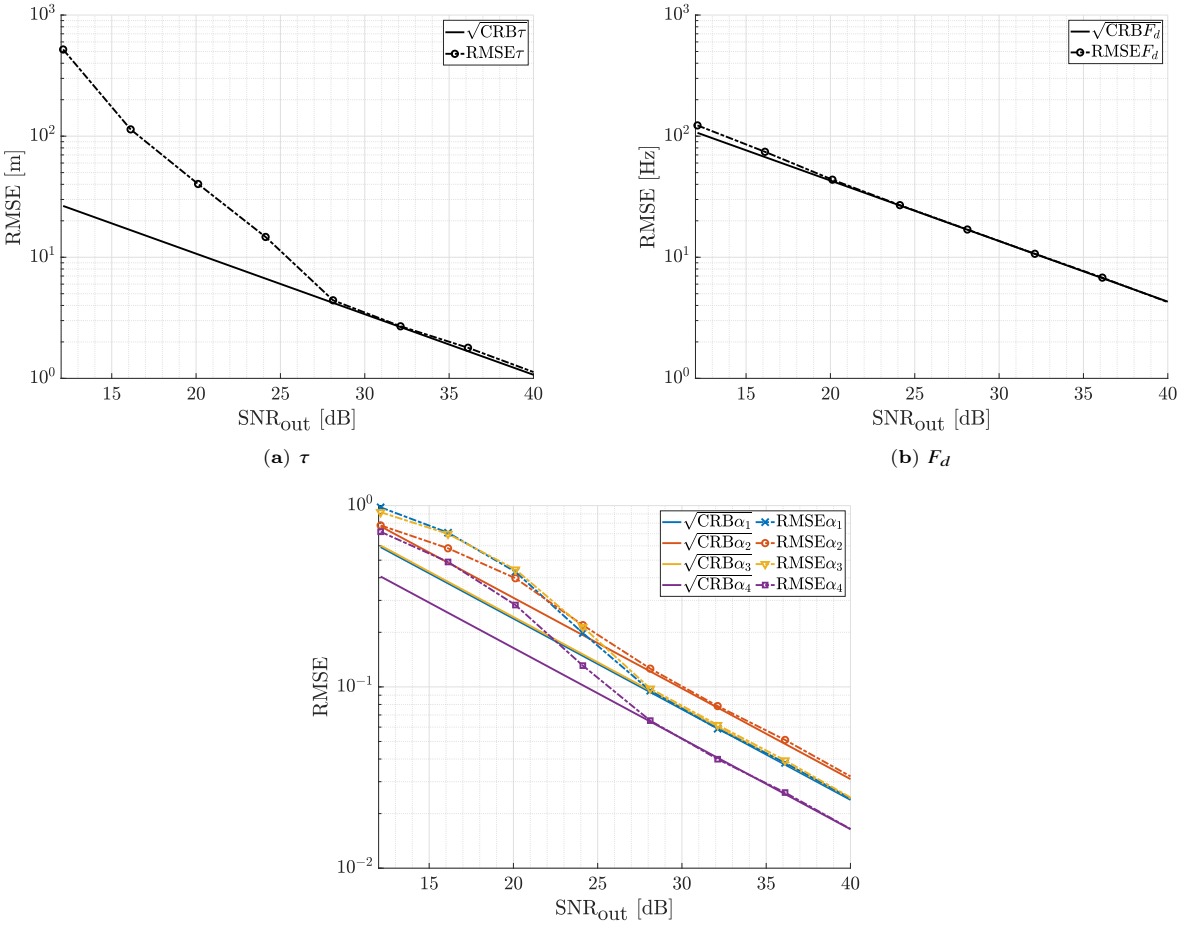

(a) τ **(b)** F_d

(c) $\boldsymbol{\alpha}$

Figure 5: Scenario #2: RMSE for the estimation of the parameters with IR-MLE(4,T_s).

and its corresponding transfer function,

$$H(f) = \sum_{p=1}^{P} \alpha_p e^{-j2\pi f\,(p-1)T_s} + \sum_{q=1}^{\infty} \alpha_{P+q} e^{-j2\pi f\,(P+q-1)T_s} = \sum_{p=1}^{P} \alpha_p e^{-j2\pi f\,(p-1)T_s}, \tag{31}$$

which is fully described with the samples $\boldsymbol{\alpha}^T = (\alpha_1, \ldots, \alpha_P)$. One can then distinguish:

- the intermediate zero coefficients, $\alpha_p = 0$, $2 \leq p \leq P-1$ which are part of the transfer function definition,
- the trailing zero coefficients, $\alpha_{P+q} = 0$, $1 \leq q$ which are not part of the transfer function.

In order to better understand the impact of under- and over shooting, the global MSE of the impulse

response is considered.

$$\mathrm{MSE}_H \ , \ E\left\{\frac{1}{F_s}\int_{-\frac{F_s}{2}}^{\frac{F_s}{2}}\left|H(f)-\widehat{H}(f)\right|^2 \mathrm{d}f\right\} = E\left\{\frac{1}{F_s}\int_{-\infty}^{\infty}\left|h(t)-\widehat{h}(t)\right|^2 \mathrm{d}t\right\} \tag{32}$$

Three cases can be thought of to evaluate (32).

- Undershooting case:

$$\widehat{H}(f) = \sum_{q=1}^{P-\ P} \widehat{\alpha}_q e^{-j2\pi f\,(q-1)T_s}, \quad 1 \leq \quad P \leq P-1, \tag{33}$$

  In this case, it can be shown that

$$\mathrm{MSE}_H = \sum_{p=1}^{P-\ P} E\left\{\left|\alpha_p-\widehat{\alpha}_p\right|^2\right\} + \sum_{q=P-\ P+1}^{P} \left|\alpha_q\right|^2, \tag{34}$$

  This is a case of misspecification which has been studied in [34, 35]. In misspecified cases, the MSE does not tend to zero remains because of the second term of (34). Besides the estimates are also affected and biased.

- Overshooting case:

$$\widehat{H}(f) = \sum_{q=1}^{P+\ P} \widehat{\alpha}_q e^{-j2\pi f\,(q-1)T_s}, \quad 1 \leq \quad P, \tag{35}$$

  Again, it can be shown that

$$\mathrm{MSE}_H = \underbrace{\sum_{p=1}^{P} E\left\{\left|\alpha_p-\widehat{\alpha}_p\right|^2\right\}}_{\text{asymptotically: } tr(\mathrm{CRB}_{\boldsymbol{\alpha}|\boldsymbol{\epsilon}})} + \sum_{q=P+1}^{P+\ P} E\left\{\left|0-\widehat{\alpha}_q\right|^2\right\}, \tag{36}$$

  Here the case is correctly specified but the estimation of the trailing zero coefficients is detrimental for two reasons

  - the estimation of the trailing zero coefficients degrade the CRB for α_p, $1 \leq p \leq P$ because increasing the number of unknown parameters increases the CRB [36].
  - the estimation of the trailing zero coefficients increases the MSE_H through the second term of (36).

  However the MSE_H converges to 0.

- Correct length case:

$$\widehat{H}(f) = \sum_{q=1}^{P} \widehat{\alpha}_q e^{-j2\pi f\,(q-1)T_s}, \qquad P \geq 1. \tag{37}$$

This case corresponds to the overshooting case (36) with $P = 0$:

$$\mathrm{MSE}_H = \underbrace{\sum_{p=1}^{P} E\left\{\left|\alpha_p - \widehat{\alpha}_p\right|^2\right\}}_{\text{asymptotically: } tr(\mathrm{CRB}_{\boldsymbol{\alpha}|\boldsymbol{\epsilon}})} . \tag{38}$$

Details on the previous results can be found in Appendix C

From this analysis, the best estimation strategy seems to be by overshooting rather than undershooting since the MSE asymptotically reduces to 0. The ideal case being having the correct impulse response length, for which the MSE_H has no additional term and the corresponding CRB is minimal.

For these reasons, test mechanisms could be thought of to either iteratively estimate the impulse response with a growing number of pulses, that is by undershooting, or to estimate it with an excessive number of pulses, or overshooting, and then evaluate the relevance of each one of the estimates, in order to see if they carry information or if they are just noise.

In the next two sections two families of procedures are presented to tackle the issue of an unknown number of pulses. The first category is iterative: it assumes a number of estimated pulses and tests if there is another pulse in the residue. The second proposed category is based on i) overshooting the number of pulses, and ii) testing how likely each estimated pulse is to be part of the impulse response.

*4.2. Iterative Procedure: $P+$*next *Test*

This first category of test assumes that P consecutive pulses have already been estimated. Then, the procedure proposed hereafter tests if there is a signal in the residual noise that results from the difference between the received signal and the estimated impulse response convoluted with a clean replica. In $P+$next, the test controls the next candidate, that is, $P+1$ whose time location is constrained at T_s after the current estimated impulse response. This test is then a simple evaluation of the likelihood that there is another source at time $\widehat{\tau} + (P+1)T_s$, the test statistic $T_{P+\mathrm{next}}$ considered is defined as

$$T_{P+\mathrm{next}} = \left| \left(\mathbf{P}^{\perp}_{\mathbf{A}_P(\widehat{\boldsymbol{\eta}})} \mathbf{y} \right)^H \mathbf{s}_{P+1}(\widehat{\boldsymbol{\eta}}) \right|^2 . \tag{39}$$

Under the null hypothesis H_0, there is no sources except the P sources already detected. Under the alternative hypothesis H_1, there is an extra source at $P+1$. This test can be written as follows:

$$H_0 : \quad T_{P+\mathrm{next}} < \text{threshold } h, \tag{40}$$

$$H_1 : \quad T_{P+\mathrm{next}} > \text{threshold } h. \tag{41}$$

Consequently, under H_0, the orthogonal projection of the data vector over the noise subspace, $\mathbf{P}^{\perp}_{\mathbf{A}_P(\widehat{\boldsymbol{\eta}})}\mathbf{y}$, is

simply noise. However, $\mathbf{s}_{P+1}(\widehat{\boldsymbol{\eta}})$ being a deterministic series of 1 and -1 of average 0 very close to the P previous signals, the test statistic $T_{P+\text{next}}$ is a combination of complex Gaussian random variables that are *dependent*. It results that this dependency reduces the variance of the orthogonal projection of $\mathbf{s}_{P+1}$ over the space of the P previous pulses, defined by $\mathbf{A}_P$. This variance is decreased by a coefficient k_σ that depends on the distance between each pulse (fixed by F_s) and the number of pulses already estimated. See Appendix D for more details to evaluate this coefficient. With k_σ evaluated, it is possible to normalize the test statistic $T_{P+\text{next}}$ to obtain a χ^2_2 distribution,

$$\left(\mathbf{P}^{\perp}_{\mathbf{A}_P(\widehat{\boldsymbol{\eta}})}\mathbf{y}\right)^H \mathbf{s}_{P+1}(\widehat{\boldsymbol{\eta}}) \xrightarrow{H_0} \left(\mathbf{P}^{\perp}_{\mathbf{A}_P(\widehat{\boldsymbol{\eta}})}\mathbf{n}\right)^H \mathbf{s}_{P+1}(\widehat{\boldsymbol{\eta}}) \sim \mathcal{CN}(0, Nk_\sigma\sigma_n^2) \quad \text{and} \quad \frac{2}{Nk_\sigma\sigma_n^2}T_{P+\text{next}} \sim \chi^2_2. \tag{42}$$

From this, one can fix the probability of false alarm (PFA) and determine the corresponding threshold h of this test,

$$\text{PFA} = P\left[\frac{2}{Nk_\sigma\sigma_n^2}T_{P+\text{next}} > h \,|\, H_0\right] = 1 - \left(1 - e^{-h/2}\right) \Leftrightarrow h = -2\log\left(\text{PFA}\right). \tag{43}$$

Based on the test definition in (40), if the test statistic is smaller than this threshold, the user will decide that there is no signal at the next time location with a given PFA.

4.2.1. Wrap-up on the Iterative Procedure

The $P+$next procedure is summarized in the Algorithm 1:

Algorithm 1: $P+$next procedure.

```
   // Initialization (T_s and threshold must be defined before)
 1 nSources ← 1;
 2 test_interrupt ← false;
   // Loop
 3 while test_interrupt is false do
 4 |   estimate ε̂^(nSources) with IR-MLE(nSources, T_s) applied to the data;
 5 |   compute T_{P+next};
 6 |   if T_{P+next} > threshold then
   |   |   // H_1 :  there is another source
 7 |   |   nSources ← nSources + 1;
 8 |   else
   |   |   // H_0 :  there is no more sources
 9 |   |   test_interrupt ← true;
10 |   end
11 end
12 return nSources, ε̂^(nSources)
```

This first test is quite simple, however, it has a few limitations: i) it focuses on one single time location, that is, if there is no energy at the next three time locations but there is one at the fourth (this is the case of intermediate zero coefficients mentioned in Section 4.1), the user might not be able to see it, ii) if the

threshold is reached, there is a possibility that the detected item is actually further, and iii) even if the test itself is simple, the overall procedure results quite time consuming because one has to re-evaluate the IR-MLE, that is, line 4 of Algorithm 1, with an increasing number of sources, which can be quite large.

4.2.2. Numerical Illustrations

In order to illustrate the $P+$next test described by the Algorithm 1, simulations are performed to evaluate, for a given PFA, the probability of detection (PD) of the correct number of sources for three SNR scenarios. The results presented in Table 1 were obtained for PFA set to 0.01 and for the scenario #1 described in 3a. 2000 runs were performed to estimate the PD defined as the percentage of runs for which the correct number of sources (4) was determined. For these good estimates, the corresponding RMSE for each unknown parameter was computed and compared with the root CRB.

Table 1: Numerical results for the $P+$next procedure with PFA = 0.01 applied to scenario #1.

SNR [dB]	PD	RMSE_τ [s]	$\sqrt{\text{CRB}_\tau}$ [s]	RMSE_{F_d} [Hz]	$\sqrt{\text{CRB}_{F_d}}$ [Hz]	MSE_H	$\sqrt{\text{CRB}_H}$
20	0.08	9.86	15.55	26.43	24.85	0.46	0.61
23	0.46	9.71	11.01	17.55	17.60	0.38	0.43
26	0.93	8.34	7.79	12.81	12.46	0.32	0.30

The range of SNR considered corresponds to the transitional area in Figure 4a where the RMSE gets closer to the root CRB. The results presented in Table 1 show that for low SNR, the PD is poor due to the noise. In this case, by computing the RMSE with the few good candidates for which the number of sources was correctly determined, this RMSE term can be below the lower bound predicted by the CRB. This is not very surprising since only a selected subset of the estimates is used whereas the CRB is computed for all possible estimates. For larger SNR, the RMSE is closer to the one obtain in simulation in Section 3.3.3, Figure 4a. To obtain the actual lower bound of the detection and estimation procedure, one would need to compute the CRB conditioned by the detection test, which is far beyond the scope of this paper. For higher SNR, the PD gets closer to 1 and all the computed RMSE tend to the corresponding CRB.

4.3. Overshoot-and-Decimate Procedures

As mentioned in the previous section, iterative approaches to determine the number of sources are known to be time consuming: the user would potentially need to run consecutive and increasingly complex estimators until reaching a satisfying number of pulses. An alternative approach is to deliberately overestimate the number of sources and try to differentiate the estimated pulses to see whether they are actual pulses or simply trailing zero coefficients. The idea is to fix a maximum number of pulses M and to apply a IR-MLE(M, T_s) for M pulses. Suppose now that there are only K actual pulses among the M estimated ones, it was shown in Section 4.1 and [37] that asymptotically, the K true values are among the M estimates. Consequently, one only needs to test each of the M pulses and discard the least relevant with an appropriate criterion.

4.3.1. Overshooting Example

First, the aim is to highlight the presence of the true values in the output of the overshooting IR-MLE(M, T_s). Figure 6 presents the output of the IR-MLE(M, T_s) looking for $M = 6$ pulses for the two scenarios presented in Figure 3a and 3b where $K = 4$. These figures were obtained by running 1000 Monte Carlo simulations and estimating systematically 6 pulses, the SNR_{out} as defined in (29) was set to 39dB. The estimated amplitudes located at their estimated delay are plotted. In these figures, one can see that for any scenario, the estimator spots the true pulses among a number of lower amplitude estimates. It then sounds reasonable to think that an adequate test on the estimated vector would filter out the non-relevant estimates.

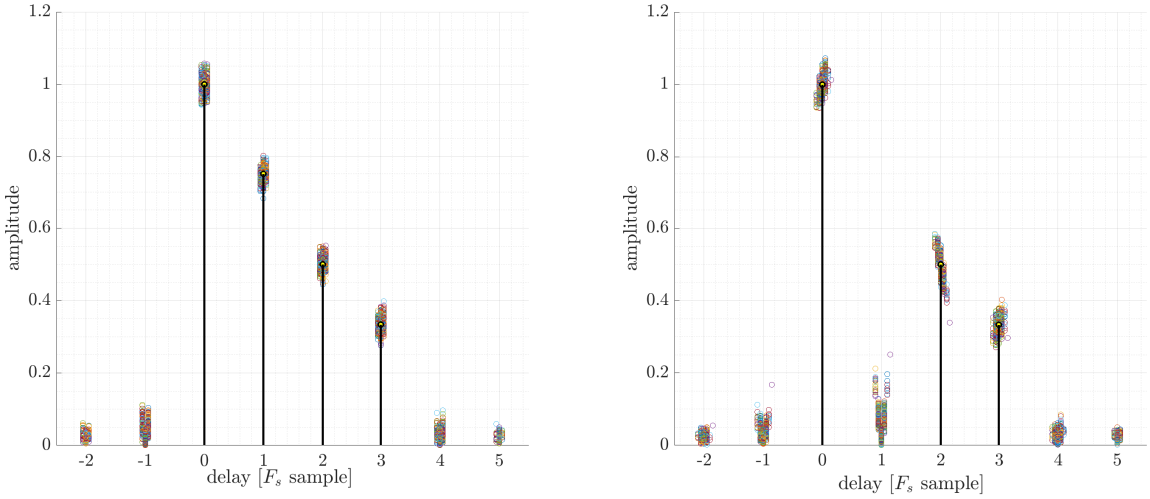

(**a**) Scenario #1 (**b**) Scenario #2

Figure 6: Output of the misspecified IR-MLE(M, T_s) ($M = 6$, $K = 4$) : (**a**) Scenario #1, (**b**) Scenario #2.

4.3.2. Chung and Mecklenbräuker Test

In order to test the relevance of each estimate with the resulting vector of estimated parameters: $\widehat{\zeta}_M^T = \left(\widehat{\tau}, \widehat{F_d}, \widehat{\boldsymbol{\rho}}_M^T, \widehat{\boldsymbol{\phi}}_M^T\right)$, one may consider the following hypothesis to be tested, as done in [37],

- H_m: the m-th pulse is null: $\rho_m = 0 \rightarrow \mathbf{y} = \sum_{p=1, p<m}^{M} \rho_p e^{j\phi_p} \mathbf{s}_p + \mathbf{n}$
- A_m: the m-th pulse is not null: $\rho_m < 0 \rightarrow \mathbf{y} = \sum_{p=1}^{M} \rho_p e^{j\phi_p} \mathbf{s}_p + \mathbf{n}$

Consequently, one can think of a likelihood ratio (LR) that would compare both hypothesis,

$$\text{LR}_m = \frac{\left\| \mathbf{P}^{\perp}_{\mathbf{A}_M} \mathbf{y} \right\|^2}{\left\| \mathbf{P}^{\perp}_{\mathbf{A}_{M-1,m}} \mathbf{y} \right\|^2}, \tag{44}$$

where $\mathbf{A}_{M-1,m} = \mathbf{A}_{M-1,m}(\widehat{\boldsymbol{\eta}})$ denotes the matrix $\mathbf{A}_M = \mathbf{A}_M(\widehat{\boldsymbol{\eta}})$ without the m-th column. This test statistic is then compared to a threshold to decide whether the m-th source should be discarded:

$$H_m: \quad \mathrm{LR}_m < \text{threshold } h, \tag{45}$$

$$A_m: \quad \mathrm{LR}_m > \text{threshold } h. \tag{46}$$

It can be shown that, under the null hypothesis H_m, LR_m has a β distribution with shape parameters 1 and $N-1$. See Appendix E for more details on the distribution derivation.

Consequently, from the cumulative distribution function of a β distribution, one can link the threshold h to a given PFA,

$$\mathrm{PFA} = P[\mathrm{LR}_m > h \,|\, \mathrm{LR}_m \sim \beta_{1,N-1}] = 1 - \frac{B_h(1,N-1)}{B(1,N-1)} = (1-h)^{N-1} \Leftrightarrow h = 1 - \mathrm{PFA}^{\frac{1}{N-1}} \tag{47}$$

where B is the beta function and B_h is the incomplete beta function.

4.3.3. Variant: Sorted Amplitudes Decimation

An intuitive extension of the Chung and Mecklenbräuker test is to order the vector of estimated pulses according to their corresponding amplitudes $\tilde{\boldsymbol{\rho}}$, where $\tilde{\boldsymbol{\rho}}_1 < \tilde{\boldsymbol{\rho}}_2 < \ldots < \tilde{\boldsymbol{\rho}}_M$. The idea is then to test each consecutive pulse from the weakest to the strongest. If the m-th is tested and tagged non-relevant, it is then removed from the vector of amplitudes $\tilde{\boldsymbol{\rho}}$. Consequently, as long as the pulses are removed, it is always the first element of the vector whose relevance is tested and the size of the projector $\mathbf{P}_{\mathbf{A}}$ is reduced. The test stops whenever there is a pulse that is considered relevant because this one is strong enough to be an actual pulse. Because the test is going from the weakest to the strongest pulse, this implies that the remaining ones will be relevant as well. This might be interesting to limit the number of tests done.

4.3.4. Wrap-up on the Overshoot-and-Decimate Procedure

The overshoot-and-decimate procedure as described in Section 4.3.2, is summarized in the Algorithm 2:

4.3.5. Numerical Illustrations

Similarly to the iterative procedure, in order to illustrate the overshoot-and-decimate procedure described in Algorithm 2, simulations are performed and the PD is evaluated for a given PFA and three SNR scenarios. The obtained results are presented in Table 2. To obtain them, the initial number of sources was set to $M = 6$, PFA was set to 0.01 and scenario #1 was considered. 2000 runs were performed to evaluate the PD. Following the Algorithm 2 structure, in the case of a correct detection of the number of pulses, the corresponding RMSE for each unknown parameters along with the root CRB are also recorded.

Algorithm 2: Overshoot-and-Decimate procedure.

```
   // Initialization (T_s, threshold and M must be defined before)
1  estimate ε̂^(M) with IR-MLE(M, T_s) applied to the data;
2  relevant_indexes ← [ ];
   // Loop to check the sources relevance
3  for m in 1 : M do
4  |  compute LR_m;
5  |  if LR_m > threshold then
   |  |  // A_m:  source m is relevant
6  |  |  relevant_indexes ← [relevant_indexes, m];
7  |  else
   |  |  // H_m:  source m is not relevant, do nothing
8  |  end
9  end
   // Last run of IR-MLE to obtain the optimal solution
10 nSources ← relevant_indexes[end] - relevant_indexes[1];
11 estimate ε̂^(nSources) with IR-MLE(nSources, T_s) applied to the data;
12 return nSources, ε̂^(nSources)
```

Table 2: Numerical results for the overshoot-and-decimate procedure with PFA = 0.01 applied to scenario #1.

SNR [dB]	PD	RMSE_τ [s]	$\sqrt{\text{CRB}_\tau}$ [s]	RMSE_{F_d} [Hz]	$\sqrt{\text{CRB}_{F_d}}$ [Hz]	MSE_H	$\sqrt{\text{CRB}_H}$
20	0.29	17.32	15.55	25.11	24.85	0.65	0.61
23	0.57	12.77	11.01	17.36	18.24	0.50	0.43
26	0.76	9.04	7.79	12.64	12.42	0.37	0.30

The overshoot-and-decimate procedure presents a poor PD for low SNR. As expected, it gets better as the SNR gets larger. For low SNR, the performance of this procedure is slightly better than the $P+$next procedure performance presented in Table 1 and the computed RMSE are close the MLE RMSE displayed in Figure 4.

5. Conclusion

In this study, the distortion of a band-limited signal due to an extended target or a reflecting surface has been modeled as a convolution between the incident signal and the impulse response of the reflecting surface. This model applies to radar, sonar and series of remote sensing scenarios. It was then shown that the received signal at the output of the Hilbert filter could be seen as a conditional signal model. A closed-form of the Cramér-Rao bound was then derived. This expression is easy-to-use because it is a function of the signal baseband samples. This CRB expression has been validated by comparing it to existing expressions, and to the corresponding maximum likelihood estimator mean square error. All the previous steps have been done assuming a known number of pulses that describe the impulse response. The question of determining this number of pulses was then addressed with first a theoretical analysis of the impact of a misspecified number

of pulses on the global impulse response MSE, and second, proposing two detection strategies adapted to the signal model under study, these strategies were illustrated with simulations to present their performance for different SNR levels. Once the number and position of pulses is correctly determined, a properly specified maximum likelihood estimator can be build in order to obtain the best estimate of the impulse response.

Acknowledgment

This work was partially supported by CNES and DGA/AID projects 2022.65.0082 and 2021.65.0070.00.470.75.01.

Appendix A. Details of the Derivation of the Fisher Information Matrix

Appendix A.1. Real and Imaginary Parts Parameterization

This section provides details on the derivation of FIM (17). From the signal model (8), the derivative of the signal w.r.t. the vector of unknown parameters excluding the noise variance $\bar{\boldsymbol{\epsilon}}^T = (\boldsymbol{\eta}^T, \alpha_1^r, \alpha_1^i, \ldots, \alpha_P^r, \alpha_P^i)$ can be expressed in a matrix form,

$$\frac{\partial}{\partial \bar{\boldsymbol{\epsilon}}} \left(\sum_{p=1}^{P} d_p(t; \boldsymbol{\eta}, \rho_p, \phi_p) \right) = \mathbf{Q}(\bar{\boldsymbol{\epsilon}}) \mathcal{D}(t; \tau) \mathbf{e}(t; \boldsymbol{\eta}), \tag{A.1}$$

where, with $p \in [1, P]$,

$$\mathbf{Q}(\bar{\boldsymbol{\epsilon}}) = \left[\begin{array}{c|c|c} j\omega_c b \boldsymbol{\alpha}^T & \mathbf{0}_{1,P} & -\boldsymbol{\alpha}^T \\ \mathbf{0}_{1,P} & -j\omega_c \boldsymbol{\alpha}^T & \mathbf{0}_{1,P} \\ \hline \boldsymbol{I}_P \otimes \begin{pmatrix} 1 \\ j \end{pmatrix} & \mathbf{0}_{2P,P} & \mathbf{0}_{2P,P} \end{array}\right], \quad \mathbf{e}(t; \boldsymbol{\eta}) = \left[\begin{array}{c|c|c} \boldsymbol{\Psi}_P(t; \boldsymbol{\eta}) & \mathbf{0}_{P,P} & \mathbf{0}_{P,P} \\ \hline \mathbf{0}_{P,P} & \boldsymbol{\Psi}_P(t; \boldsymbol{\eta}) & \mathbf{0}_{P,P} \\ \hline \mathbf{0}_{P,P} & \mathbf{0}_{P,P} & \boldsymbol{\Psi}_P(t; \boldsymbol{\eta}) \end{array}\right], \tag{A.2}$$

$$\mathcal{D}(t; \tau) = \left[\begin{array}{c} \vdots \\ s(t - \tau_p) \\ \vdots \\ \hline \vdots \\ (t - \tau_p) s(t - \tau_p) \\ \vdots \\ \hline \vdots \\ s^{(1)}(t - \tau_p) \\ \vdots \end{array}\right], \quad \boldsymbol{\Psi}_P(t; \boldsymbol{\eta}) = \begin{bmatrix} \ddots & 0 & 0 \\ 0 & e^{-j\omega_c b(t-\tau_p)} & 0 \\ 0 & 0 & \ddots \end{bmatrix}. \tag{A.3}$$

where $\otimes$ denotes the Kronecker product.

Therefore the derivative of the vector $(\mathbf{A}_P\boldsymbol{\alpha})^T$ ($t = nT_s$, with samples $N_1 \leq n \leq N_2$) w.r.t. $\bar{\boldsymbol{\epsilon}}$ is

$$\begin{aligned}\frac{\partial\,(\mathbf{A}_P\boldsymbol{\alpha})^T}{\partial\bar{\boldsymbol{\epsilon}}} &= \left[\begin{array}{ccc} \dots & \frac{\partial}{\partial\bar{\epsilon}}\left(\sum_{p=1}^{P} d_p(nT_s;\boldsymbol{\eta},\rho_p,\phi_p)\right) & \dots \end{array}\right] = \left[\begin{array}{ccc} \dots & \mathbf{Q}(\bar{\boldsymbol{\epsilon}})\mathcal{D}(nT_s;\bar{\boldsymbol{\epsilon}})\mathbf{e}(nT_s;\bar{\boldsymbol{\epsilon}}) & \dots \end{array}\right] \\ &= \mathbf{Q}(\bar{\boldsymbol{\epsilon}})\left[\begin{array}{ccc} \dots & \mathcal{D}(nT_s;\bar{\boldsymbol{\epsilon}})\mathbf{e}(nT_s;\bar{\boldsymbol{\epsilon}}) & \dots \end{array}\right]. \end{aligned} \tag{A.4}$$

Then, remembering the following properties,

$$\frac{\partial\,(\mathbf{A}_P\boldsymbol{\alpha})^H}{\partial\bar{\boldsymbol{\epsilon}}^T} = \left(\frac{\partial\,(\mathbf{A}_P\boldsymbol{\alpha})^T}{\partial\bar{\boldsymbol{\epsilon}}}\right)^*,\ \frac{\partial\,(\mathbf{A}_P\boldsymbol{\alpha})}{\partial\bar{\boldsymbol{\epsilon}}^T} = \left(\frac{\partial\,(\mathbf{A}_P\boldsymbol{\alpha})^T}{\partial\bar{\boldsymbol{\epsilon}}}\right)^T, \tag{A.5}$$

one can write that

$$\frac{\partial\,(\mathbf{A}_P\boldsymbol{\alpha})^H}{\partial\bar{\boldsymbol{\epsilon}}^T}\frac{\partial\,(\mathbf{A}_P\boldsymbol{\alpha})}{\partial\bar{\boldsymbol{\epsilon}}^T} = \left(\mathbf{Q}(\bar{\boldsymbol{\epsilon}})\left(\sum_{n=N_1}^{N_2}\mathcal{D}(nT_s;\bar{\boldsymbol{\epsilon}})\mathcal{D}(nT_s;\bar{\boldsymbol{\epsilon}})^H\right)\mathbf{Q}(\bar{\boldsymbol{\epsilon}})^H\right)^*. \tag{A.6}$$

If one evaluates the limit when N_1 and N_2 tend to infinity:

$$\lim_{(N_1,N_2)\to(-\infty,+\infty)} T_s\sum_{n=N_1}^{N_2}\mathcal{D}(nT_s;\bar{\boldsymbol{\epsilon}})\mathcal{D}(nT_s;\bar{\boldsymbol{\epsilon}})^H = \int_{-\infty}^{+\infty}\mathcal{D}(t;\bar{\boldsymbol{\epsilon}})\mathcal{D}(t;\bar{\boldsymbol{\epsilon}})^H\mathrm{d}t = \left[\begin{array}{ccc} \mathbf{W}_1^\delta & \mathbf{W}_2^{\delta H} & \mathbf{W}_3^{\delta H} \\ \mathbf{W}_2^\delta & \mathbf{W}_{2,2}^\delta & \mathbf{W}_4^{\delta H} \\ \mathbf{W}_3^\delta & \mathbf{W}_4^\delta & \mathbf{W}_{3,3}^\delta \end{array}\right], \tag{A.7}$$

where, for p and q in $[1, P]$

$$\left[\mathbf{W}_1^\delta\right]_{p,q} = \int_{\mathsf{R}} s(t-\tau_p)s(t-\tau_q)^*\mathrm{d}t \tag{A.8}$$

$$\left[\mathbf{W}_2^\delta\right]_{p,q} = \int_{\mathsf{R}} (t-\tau_p)s(t-\tau_p)s(t-\tau_q)^*\mathrm{d}t \tag{A.9}$$

$$\left[\mathbf{W}_3^\delta\right]_{p,q} = \int_{\mathsf{R}} s_p^{(1)}(t-\tau_p)s(t-\tau_q)^*\mathrm{d}t \tag{A.10}$$

$$\left[\mathbf{W}_4^\delta\right]_{p,q} = \int_{\mathsf{R}} (t-\tau_q)s^{(1)}(t-\tau_p)s(t-\tau_q)^*\mathrm{d}t \tag{A.11}$$

$$\left[\mathbf{W}_{2,2}^\delta\right]_{p,q} = \int_{\mathsf{R}} (t-\tau_p)(t-\tau_q)s(t-\tau_p)s(t-\tau_q)\mathrm{d}t \tag{A.12}$$

$$\left[\mathbf{W}_{3,3}^\delta\right]_{p,q} = \int_{\mathsf{R}} s^{(1)}(t-\tau_p)s^{(1)}(t-\tau_q)\mathrm{d}t \tag{A.13}$$

As an example, the details of the derivation of the first term (A.8) can be found as follows, the derivation is based on the properties of the Fourier transform over the hermitian product.

$$\begin{aligned}\left[\mathbf{W}_1^{\delta}\right]_{p,q} &= \int_{\mathsf{R}} s(t-\tau_p)s(t-\tau_q)^* \mathrm{d}t \\ &= \int_{\mathsf{R}} s(u-(p-q)T_s)s(u)^* \mathrm{d}u \\ &= \int_{-\frac{F_s}{2}}^{\frac{F_s}{2}} S(f)e^{-j2\pi f(p-q)T_s} S(f)^* \mathrm{d}f\end{aligned}$$

and, if one sees the sum definition of the Fourier transform (1) as a matrices product,

$$\begin{aligned}\left[\mathbf{W}_1^{\delta}\right]_{p,q} &= \frac{1}{F_s}\int_{-\frac{1}{2}}^{\frac{1}{2}} \left(\mathbf{s}^T \boldsymbol{\nu}(f)^*\right) e^{-j2\pi f(p-q)} \left(\mathbf{s}^H \boldsymbol{\nu}(f)\right) \mathrm{d}f \\ &= \frac{1}{F_s}\mathbf{s}^H \mathbf{V}^{,0}(p-q)\mathbf{s}\end{aligned} \tag{A.14}$$

with

$$\mathbf{s} = \begin{pmatrix} \dots & s(nT_s) & \dots \end{pmatrix}^T_{N_1 \le n \le N_2} \tag{A.15}$$

$$\boldsymbol{\nu}(f) = \begin{pmatrix} \dots & e^{j2\pi f n} & \dots \end{pmatrix}^T_{N_1 \le n \le N_2} \tag{A.16}$$

$$\mathbf{V}^{,0}(n) = \int_{-\frac{1}{2}}^{\frac{1}{2}} \boldsymbol{\nu}(f)\boldsymbol{\nu}^H(f)e^{-j2\pi f n}\mathrm{d}f \tag{A.17}$$

$$\left[\mathbf{V}^{,0}(n)\right]_{k,l} = \int_{-\frac{1}{2}}^{\frac{1}{2}} e^{j2\pi f(k-l-n)}\mathrm{d}f = \mathrm{sinc}(k-l-n) = \begin{cases} 1 & k-l=n, \\ 0 & \text{else} \end{cases} \tag{A.18}$$

The other $\mathbf{W}^{\delta}$ terms are similarly derived, the details of these derivations can be found in [38, Sec. 1]. Series of additional variables are used to obtain the results presented in (19), they can be found below.

$$\mathbf{D} = \begin{pmatrix} \dots & n & \dots \end{pmatrix}^T_{N_1 \le n \le N_2} \tag{A.19}$$

$$\mathbf{V}^{,1}(n) = j2\pi \int_{-\frac{1}{2}}^{\frac{1}{2}} f\boldsymbol{\nu}(f)\boldsymbol{\nu}^H(f)e^{-j2\pi f n}\mathrm{d}f \tag{A.20}$$

$$\left[\mathbf{V}^{,1}(n)\right]_{k,l} = j2\pi \int_{-\frac{1}{2}}^{\frac{1}{2}} f e^{j2\pi f(k-l-n)}\mathrm{d}f = \begin{cases} 0 & k-l=n, \\ (-1)^{|k-l-n|}/(k-l-n) & \text{else} \end{cases} \tag{A.21}$$

$$\mathbf{V}^{,2}(n) = 4\pi^2 \int_{-\frac{1}{2}}^{\frac{1}{2}} f^2\boldsymbol{\nu}(f)\boldsymbol{\nu}^H(f)e^{-j2\pi f n}\mathrm{d}f \tag{A.22}$$

$$\left[\mathbf{V}^{,2}\left(\frac{\tau}{T_s}\right)\right]_{k,l} = 4\pi^2 \int_{-\frac{1}{2}}^{\frac{1}{2}} f^2 e^{j2\pi f(k-l-n)} \mathrm{d}f = \begin{cases} \pi^2/3 & k-l=n, \\ (-1)^{|k-l-n|} 2/(k-l-n)^2 & \text{else} \end{cases} \tag{A.23}$$

Appendix A.2. Amplitude and Phase Parameterization

In order to obtain the expression of the FIM for the vector of parameters $\bar{\boldsymbol{\zeta}}^T = (\boldsymbol{\eta}^T, \boldsymbol{\rho}^T, \boldsymbol{\phi}^T)$, the only difference is in the derivative of the signal w.r.t. $\bar{\boldsymbol{\zeta}}$. Again, this derivative can be expressed in a matrix form,

$$\frac{\partial}{\partial \bar{\boldsymbol{\zeta}}} \left(\sum_{p=1}^{P} d_p(t; \boldsymbol{\eta}, \rho_p, \phi_p) \right) = \mathbf{Q}(\bar{\boldsymbol{\zeta}}) \mathcal{D}(t;\tau) \mathbf{e}(t;\boldsymbol{\eta}), \tag{A.24}$$

where, with $p \in [1, P]$,

$$\mathbf{Q}(\bar{\boldsymbol{\zeta}}) = \left[\begin{array}{c|c|c} j\omega_c b\boldsymbol{\alpha}^T & \mathbf{0}_{1,P} & -\boldsymbol{\alpha}^T \\ \mathbf{0}_{1,P} & -j\omega_c \boldsymbol{\alpha}^T & \mathbf{0}_{1,P} \\ \hline \boldsymbol{\Phi}_P & \mathbf{0}_{P,P} & \mathbf{0}_{P,P} \\ \hline \mathbf{diag}(j\boldsymbol{\rho})\boldsymbol{\Phi}_P & \mathbf{0}_{P,P} & \mathbf{0}_{P,P} \end{array}\right], \boldsymbol{\Phi}_P = \left[\begin{array}{ccc} \ddots & 0 & 0 \\ 0 & e^{j\phi_p} & 0 \\ 0 & 0 & \ddots \end{array}\right], \tag{A.25}$$

with $\mathbf{e}(t;\boldsymbol{\eta})$ defined in (A.2), $\mathcal{D}(t;\tau)$ defined in (A.3) and $\mathbf{diag}(j\boldsymbol{\rho})$ the square diagonal matrix with its diagonal equal to $j\boldsymbol{\rho}$.

Appendix B. Note on the Implementation of the Maximum Likelihood Estimator

This appendix further develops the projector term to be maximized to obtain the estimated vector $\widehat{\boldsymbol{\eta}}$. If one considers the expression of the projection in (26):

$$\left\|\mathbf{P}_{\mathbf{A}_P}\mathbf{y}\right\|^2 = \mathbf{y}^H \mathbf{P}_{\mathbf{A}_P}\mathbf{y} = \left(\mathbf{A}_P^H \mathbf{y}\right)^H \left(\mathbf{A}_P^H \mathbf{A}_P\right)^{-1} \mathbf{A}_P^H \mathbf{y} \tag{B.1}$$

For a given sampling frequency F_s, the inverse term in (B.1) depends only on P, the number of sources considered in the estimation:

$$\mathbf{A}_P^H \mathbf{A}_P = \left[\begin{array}{c} \mathbf{s}_1^H \\ \vdots \\ \mathbf{s}_P^H \end{array}\right] [\mathbf{s}_1, \ \ldots \ , \mathbf{s}_P] \,. \tag{B.2}$$

It can then be pre-computed and stored in memory without need of re-evaluating it.

The term $\mathbf{A}_P^H \mathbf{y}$ in (B.1) is the one that directly depends on the parameters to be estimated.

$$\mathbf{A}_P^H \mathbf{y} = \begin{bmatrix} \mathbf{s}_1^H \\ \vdots \\ \mathbf{s}_P^H \end{bmatrix} \mathbf{y} \tag{B.3}$$

Therefore,

$$\left[\mathbf{A}_P^H \mathbf{y}\right]_p = \mathbf{s}_p^H \mathbf{y} = \sum_{n=N_1}^{N_2} s(nT_s - \tau_p)^* y(nT_s) e^{j\omega_c b(nT_s - \tau_p)} \tag{B.4}$$

Consequently,

$$\lim_{(N_1,N_2)\to(-\infty,+\infty)} \left[\mathbf{A}_P^H \mathbf{y}\right]_p = F_s \int_{\mathsf{R}} s(t-\tau_p)^* y(t) e^{j\omega_c b(t-\tau_p)} \mathrm{d}t = R_{y,s}(\tau_p, b), \tag{B.5}$$

where $R_{y,s}(\tau, b)$ is the ambiguity function between the received signal and the clean replica s, this function is easily computed for a range of delay τ and Doppler stretch b with Fourier transforms. The product (B.3) can then be written as follows:

$$\lim_{(N_1,N_2)\to(-\infty,+\infty)} \mathbf{A}_P^H \mathbf{y} = \begin{bmatrix} F_s R_{y,s}(\tau, b) \\ \vdots \\ F_s R_{y,s}(\tau + (P-1)T_s, b) \end{bmatrix} \tag{B.6}$$

which is a vector easy to construct since each element is a shifted replica of the precedent one. With these considerations, the search of the maximum of a P-source criterion reduces to a traditional search over a delay-Doppler grid.

Appendix C. Details on the $\mathrm{MSE}_{\boldsymbol{H}}$ for Under- and Overshooting Cases

First recall that

$$\int_{-\frac{F_s}{2}}^{\frac{F_s}{2}} e^{-j2\pi f p T_s} \left(e^{-j2\pi f q T_s}\right)^* \mathrm{d}f = \delta_p^q F_s. \tag{C.1}$$

For the undershooting case:

$$\int_{-\frac{F_s}{2}}^{\frac{F_s}{2}} \left|H(f) - \widehat{H}(f)\right|^2 \mathrm{d}f = \int_{-\frac{F_s}{2}}^{\frac{F_s}{2}} \left| \sum_{p=1}^{P} \alpha_p e^{-j2\pi f (p-1)T_s} - \sum_{q=1}^{P_-} \widehat{\alpha}_q e^{-j2\pi f (q-1)T_s} \right|^2 \mathrm{d}f \tag{C.2}$$

$$= \int_{-\frac{F_s}{2}}^{\frac{F_s}{2}} \left| \sum_{p=1}^{P_-} \left(\alpha_p - \widehat{\alpha}_p\right) e^{-j2\pi f (p-1)T_s} + \sum_{q=P_-\ P+1}^{P} \alpha_q e^{-j2\pi f (q-1)T_s} \right|^2 \mathrm{d}f \tag{C.3}$$

$$= \sum_{p=1}^{P_-} \left|\alpha_p - \widehat{\alpha}_p\right|^2 + \sum_{q=P_-\ P+1}^{P} \left|\alpha_q\right|^2 \quad \text{using (C.1)}, \tag{C.4}$$

which leads to (34).

Now regarding the overshooting case,

$$\int_{-\frac{F_s}{2}}^{\frac{F_s}{2}} \left|H(f) - \widehat{H}(f)\right|^2 \mathrm{d}f = \int_{-\frac{F_s}{2}}^{\frac{F_s}{2}} \left|\sum_{p=1}^{P} \alpha_p e^{-j2\pi f\,(p-1)T_s} - \sum_{q=1}^{P+\ P} \widehat{\alpha}_q e^{-j2\pi f\,(q-1)T_s}\right|^2 \mathrm{d}f \tag{C.5}$$

$$= \int_{-\frac{F_s}{2}}^{\frac{F_s}{2}} \left|\sum_{p=1}^{P} \left(\alpha_p - \widehat{\alpha}_p\right) e^{-j2\pi f\,(p-1)T_s} - \sum_{q=P+1}^{P+\ P} \widehat{\alpha}_q e^{-j2\pi f\,(q-1)T_s}\right|^2 \mathrm{d}f \tag{C.6}$$

$$= \sum_{p=1}^{P} \left|\alpha_p - \widehat{\alpha}_p\right|^2 + \sum_{q=P+1}^{P+\ P} \left|0 - \widehat{\alpha}_q\right|^2, \tag{C.7}$$

which leads to (36).

Appendix D. $P+$next Correlation Coefficient

Let one consider a study case: GPS L1 C/A. The auto-correlation function is known and can be modelled by a zero-centered triangle. One can then assume that the normalized cross-correlation between $\mathbf{s}_P$ and $\mathbf{s}_{P+1}$ is simply: $\mathbf{s}_P^H \mathbf{s}_{P+p} = 1 - pF_0/F_s$ where F_0 is the GPS L1 C/A chip rate, equal to 1.023 MHz. Then, if one considers the case with $P = 2$ sources already detected and no other remaining source (H_0):

$$\mathbf{P}_{\mathbf{A}_2}\mathbf{s}_3 = \mathbf{A}_2 \left(\mathbf{A}_2^H \mathbf{A}_2\right)^{-1} \mathbf{A}_2^H \mathbf{s}_3 = \begin{bmatrix} \mathbf{s}_1 & \mathbf{s}_2 \end{bmatrix} \begin{bmatrix} \mathbf{s}_1^H\mathbf{s}_1 & \mathbf{s}_1^H\mathbf{s}_2 \\ \mathbf{s}_2^H\mathbf{s}_1 & \mathbf{s}_2^H\mathbf{s}_2 \end{bmatrix}^{-1} \begin{bmatrix} \mathbf{s}_1^H\mathbf{s}_3 \\ \mathbf{s}_2^H\mathbf{s}_3 \end{bmatrix} \tag{D.1}$$

Then with the approximated triangular shape and assuming that $F_s/F_0 \gg 1$, one can get

$$\mathbf{P}^{\perp}_{\mathbf{A}_2}\mathbf{s}_3 \approx \mathbf{s}_3 - \left(1 - \frac{F_0}{F_s}\right)\mathbf{s_2} + \frac{F_0}{2F_s}\mathbf{s_1}. \tag{D.2}$$

And for F_s large enough, this is no longer a series of $+1$ and -1 because of the cross-correlation between close-in-time signals. Figure D.7 shows an example for $F_s = 8F_0$: the variance of $\mathbf{s}_3$ is 1 but the variance of its orthogonal projection is now 0.2336. There is then a given correlation coefficient k_σ that depends on F_s, the pseudo-random noise code, the number of signals and the distance between the consecutive pulses considered. This coefficient directly determines the distribution under H_0 and is needed to set the threshold for a given probability of false alarm. However it is difficult to anticipate k_σ, as it can be seen in the following table D.3. Consequently, k_σ needs to be evaluated during the detection test.

Table D.3: Exemples of k_σ for GPS L1 C/A with $P = 2$.

F_s/F_0	2	4	8	12
k_σ	0.6673	0.4290	0.2336	0.1596

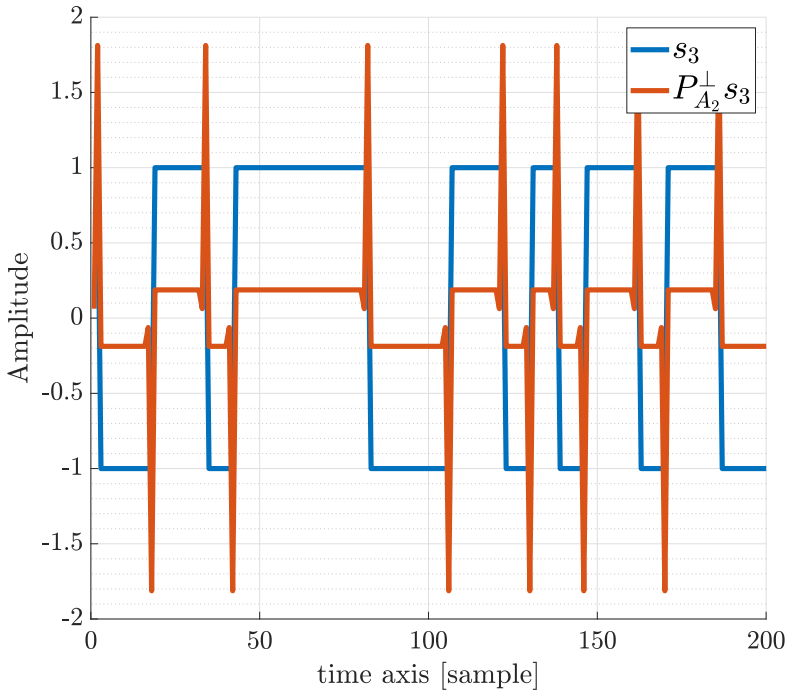

Figure D.7: Projection of $\mathbf{s}_{P+1}$ on the space spanned by the columns of $\mathbf{A}_P$, $P = 2$, $F_s = 8F_0$.

Appendix E. Chung and Mecklenbräuker Likelihood Ratio Distribution Derivation

The orthogonal projector over the space defined by the column of $\mathbf{A}_M$ can be separated into two orthogonal projectors. One over the subspace defined by $M-1$ columns (omitting the m-th component) and the other, which is naturally the projection upon the subspace defined by the m-th column, orthogonalized:

$$\mathbf{P}_{\mathbf{A}_M} = \mathbf{P}_{\mathbf{A}_{M-1,m}} + \mathbf{P}_{\left(\mathbf{P}^{\perp}_{\mathbf{A}_{M-1,m}} \mathbf{s}_m\right)} \tag{E.1}$$

Proof. See [38, Sec. 2] for more details.

Consequently, the likelihood ratio defined in (44) can be reorganized using the orthogonal decomposition (E.1):

$$\mathrm{LR}_m = \frac{\left\|\mathbf{P}^{\perp}_{\mathbf{A}_M}\mathbf{y}\right\|^2}{\left\|\mathbf{P}^{\perp}_{\mathbf{A}_{M-1,m}}\mathbf{y}\right\|^2} = \frac{\left\|\mathbf{P}^{\perp}_{\mathbf{A}_{M-1,m}}\mathbf{y}\right\|^2 - \left\|\mathbf{P}_{\left(\mathbf{P}^{\perp}_{\mathbf{A}_{M-1,m}}\mathbf{s}_m\right)}\mathbf{y}\right\|^2}{\left\|\mathbf{P}^{\perp}_{\mathbf{A}_{M-1,m}}\mathbf{y}\right\|^2} = 1 - \frac{\left|\mathbf{s}_m^H \mathbf{P}^{\perp}_{\mathbf{A}_{M-1,m}}\mathbf{y}\right|^2}{\left\|\mathbf{P}^{\perp}_{\mathbf{A}_{M-1,m}}\mathbf{s}_m\right\|^2 \left\|\mathbf{P}^{\perp}_{\mathbf{A}_{M-1,m}}\mathbf{y}\right\|^2} \tag{E.2}$$

Under the H_m hypothesis, the m-th component is not relevant. In that case the numerator $\left|\mathbf{s}_m^H \mathbf{P}^{\perp}_{\mathbf{A}_{M-1,m}}\mathbf{y}\right|^2$ has the same probability density function as in (42), the first norm of the denominator $\left\|\mathbf{P}^{\perp}_{\mathbf{A}_{M-1,m}}\mathbf{s}_m\right\|^2$ is an

attenuated version of the vector $\mathbf{s}_m$ as detailed in Appendix D and the last norm is the norm of the residual noise. In short:

$$\mathrm{LR}_m \xrightarrow{H_m} 1 - \frac{\overbrace{\left|\mathbf{s}_m^H \mathbf{P}^{\perp}_{\mathbf{A}_{M-1,m}} \mathbf{y}\right|^2}^{\sim \chi_2^2(0, N k_\sigma \sigma_n^2/2)}}{\underbrace{\left\|\mathbf{P}^{\perp}_{\mathbf{A}_{M-1,m}} \mathbf{s}_m\right\|^2}_{=N k_\sigma} \underbrace{\left\|\mathbf{P}^{\perp}_{\mathbf{A}_{M-1,m}} \mathbf{y}\right\|^2}_{\sim \chi_{2N}^2(0, \sigma_n^2/2)}} \tag{E.3}$$

Now, considering the fractional component of this expression:

$$\mathrm{LR}_m \sim \frac{\chi_2^2}{\chi_{2N}^2} = \frac{\chi_2^2}{\chi_2^2 + \chi_{2(N-1)}^2} = \beta_{1,N-1} \tag{E.4}$$

which has a known probability density function and which allows to compute a desired probability of false alarm.

References

[1] M. Irsigler, J. A. Avila-Rodriguez, G. W. Hein, Criteria for GNSS Multipath Performance Assessment, in: Proceedings of the 18th International Technical Meeting of the Satellite Division of The Institute of Navigation (ION GNSS 2005), 2005, pp. 2166–2177.

[2] T. Mei, A. Mertins, M. Kallinger, Room Impulse Response Reshaping/Shortening Based on Least Mean Squares Optimization with Infinity Norm Constraint, in: 2009 16th International Conference on Digital Signal Processing, 2009, pp. 1–6. doi:10.1109/ICDSP.2009.5201237.

[3] C. E. R. Fernandes, P. Comon, G. Favier, Blind Identification of MISO-FIR Channels, Signal Processing 90 (2) (2010) 490–503. doi:10.1016/j.sigpro.2009.07.023.

[4] Y. Huang, J. Benesty (Eds.), Audio Signal Processing for Next-Generation Multimedia Communication Systems, Springer, Boston, MA, 2004.

[5] V. U. Zavorotny, A. G. Voronovich, Scattering of GPS Signals from the Ocean with Wind Remote Sensing Application, IEEE Transactions on Geoscience and Remote Sensing 38 (2) (2000) 951–964. doi:10.1109/36.841977.

[6] S. F. Cotter, B. D. Rao, Sparse Channel Estimation Via Matching Pursuit With Application to Equalization, IEEE Transactions on Communications 50 (3) (2002) 374–377. doi:10.1109/26.990897.

[7] P. Das, J. Vilà-Valls, F. Vincent, L. Davain, E. Chaumette, A New Compact Delay, Doppler Stretch and Phase Estimation CRB with a Band-Limited Signal for Generic Remote Sensing Applications, Remote Sensing 12 (18) (2020) 2913.

[8] H. McPhee, L. Ortega, J. Vilà-Valls, E. Chaumette, Accounting for Acceleration - Signal Parameters Estimation Performance Limits in High Dynamics Applications, IEEE Transactions on Aerospace and Electronic Systems (Early Access) (2022) 1–13doi:10.1109/TAES.2022.3189611.

[9] D. Medina, L. Ortega, J. Vilà-Valls, P. Closas, F. Vincent, E. Chaumette, A New Compact CRB for Delay, Doppler and Phase Estimation - Application to GNSS SPP & RTK Performance Characterization, IET Radar, Sonar & Navigationdoi:10.1049/iet-rsn.2020.0168.

[10] L. Ortega, J. Vilà-Valls, E. Chaumette, Insights on the Estimation Performance of GNSS-R Coherent and Non-Coherent Processing Schemes, IEEE Geoscience and Remote Sensing Letters 19 (2022) 1–5. doi:10.1109/LGRS.2021.3079579.

[11] C. Lubeigt, L. Ortega, J. Vilà-Valls, L. Lestarquit, E. Chaumette, Joint Delay-Doppler Estimation Performance in a Dual Source Context, Remote Sensing 12 (23) (2020) 3894. doi:10.3390/rs12233894.

[12] M. Gustafsson, S. Nordebo, Cramér-Rao Lower Bounds for Inverse Scattering Problems of Multilayer Structures, Inverse Problems 22 (4) (2006) 1359.

[13] T. Zhao, T. Huang, Cramer-Rao Lower Bounds for the Joint Delay-Doppler Estimation of an Extended Target, IEEE Transactions on Signal Processing 64 (6) (2016) 1562–1573.

[14] N. Garcia, A. Fascista, A. Coluccia, H. Wymeersch, C. Aydogdu, R. Mendrzik, G. Seco-Granados, Cramér-Rao Bound Analysis of Radars for Extended Vehicular Targets With Known and Unknown Shape, IEEE Transactions on Signal Processing 70 (2022) 3280–3295. doi:10.1109/TSP.2022.3183853.

[15] P. Stoica, A. Nehorai, Performance Study of Conditional and Unconditional Direction of Arrival Estimation, IEEE Trans. Acoust., Speech, Signal Process. 38 (10) (1990) 1783–1795.

[16] A. Renaux, P. Forster, E. Chaumette, P. Larzabal, On the High-SNR Conditional Maximum-Likelihood Estimator Full Statistical Characterization, IEEE Trans. Signal Process. 54 (12) (2006) 4840 – 4843.

[17] M. Wax, T. Kailath, Detection of signals by information theoretic criteria, IEEE Transactions on Acoustics, Speech, and Signal Processing 33 (2) (1985) 387–392. doi:10.1109/TASSP.1985.1164557.

[18] H. Akaike, A New Look at the Statistical Model Identification, IEEE Transactions on Automatic Control 19 (6) (1974) 716–723. doi:10.1109/TAC.1974.1100705.

[19] M. Wax, I. Ziskind, Detection of the number of coherent signals by the MDL principle, IEEE Transactions on Acoustics, Speech, and Signal Processing 37 (8) (1989) 1190–1196. doi:10.1109/29.31267.

[20] J. Rissanen, Modeling by Shortest Data Description, Automatica 14 (5) (1978) 465–471.

[21] K. M. Wong, Q.-T. Zhang, J. P. Reilly, P. C. Yip, On Information Theoretic Criteria for Determining the Number of Signals in High Resolution Array Processing, IEEE Transactions on Acoustics, Speech, and Signal Processing 38 (11) (1990) 1959–1971. doi:10.1109/29.103097.

[22] R. F. Brcich, A. M. Zoubir, P. Pelin, Detection of Sources Using Bootstrap Techniques, IEEE Transactions on Signal Processing 50 (2) (2002) 206–215.

[23] P.-J. Chung, J. F. Bohme, C. F. Mecklenbräuker, A. O. Hero, Detection of the Number of Signals Using the Benjamini-Hochberg Procedure, IEEE Transactions on Signal Processing 55 (6) (2007) 2497–2508. doi:10.1109/TSP.2007.893749.

[24] Y. Benjamini, Y. Hochberg, Controlling the False Discovery Rate: A Practical and Powerful Approach to Multiple Testing, Journal of the Royal Statistical Society: Series B (Methodological) 57 (1) (1995) 289–300.

[25] S. Kritchman, B. Nadler, Non-Parametric Detection of the Number of Signals: Hypothesis Testing and Random Matrix Theory, IEEE Transactions on Signal Processing 57 (10) (2009) 3930–3941.

[26] V. Garg, I. Santamaria, D. Ramirez, L. L. Scharf, Subspace Averaging and Order Determination for Source Enumeration, IEEE Transactions on Signal Processing 67 (11) (2019) 3028–3041.

[27] M. Wax, A. Adler, Detection of the Number of Signals by Signal Subspace Matching, IEEE Transactions on Signal Processing 69 (2021) 973–985. doi:10.1109/TSP.2021.3053495.

[28] D. W. Ricker, Echo Signal Processing, Kluwer Academic, Springer, New York, USA, 2003.

[29] H. L. Van Trees, Part III: Radar-Sonar Signal Processing and Gaussian Signals in Noise, Detection, Estimation, and Modulation Theory, Wiley, 2001.

[30] S. M. Kay, Fundamentals of Statistical Signal Processing: Estimation Theory, Prentice-Hall, Englewood Cliffs, New Jersey, USA, 1993.

[31] B. Ottersten, M. Viberg, P. Stoica, A. Nehorai, Exact and Large Sample Maximum Likelihood Techniques for Parameter Estimation and Detection in Array Processing, in: S. Haykin, J. Litva, T. J. Shepherd (Eds.), Radar Array Processing, Springer-Verlag, Heidelberg, 1993, Ch. 4, pp. 99–151.

[32] U.S. Goverment, Interface Specification IS-GPS-200 Navstar GPS Space/Segment/Navigation User Interface, Tech. rep. (2019).

[33] E. Kaplan, C. Hegarty, Understanding GPS/GNSS: Principle and Applications, 3rd Edition, Artech House, 2017.

[34] S. Fortunati, F. Gini, M. S. Greco, C. D. Richmond, Performance Bounds for Parameter Estimation under Misspecified Models: Fundamental Findings and Applications, IEEE Signal Processing Magazine 34 (6) (2017) 142–157. doi:10.1109/MSP.2017.2738017.

[35] C. D. Richmond, L. L. Horowitz, Parameter Bounds on Estimation Accuracy Under Model Misspecification, IEEE Transactions on Signal Processing 63 (9) (2015) 2263–2278. doi:10.1109/TSP.2015.2411222.

[36] T. Menni, E. Chaumette, P. Larzabal, Reparameterization and Constraints for CRB: Duality and a Major Inequality for System Analysis and Design in the Asymptotic Region, in: 2012 IEEE International Conference on Acoustics, Speech and Signal Processing (ICASSP), 2012, pp. 3545–3548.

[37] P.-J. Chung, C. F. Mecklenbräuker, Deterministic ML Estimation for Unknown Numbers of Signals, in: EUSIPCO, 2008, pp. 1–5.

[38] C. Lubeigt, L. Ortega, J. Vilà-Valls, E. Chaumette, Details on Impulse Response Estimation and Size Determination (2022).